

Boosting Crop Classification by Hierarchically Fusing Satellite, Rotational, and Contextual Data

Valentin Barriere^{1,2,*}, Martin Claverie^{2,*}, Maja Schneider³,
Guido Lemoine², Raphaël d’Andrimont²

¹ *Centro Nacional de Inteligencia Artificial (CENIA), Santiago, Chile*

² *European Commission, Joint Research Centre (JRC), Ispra, Italy*

³ *Technical University of Munich, Munich, Germany*

* Shared first authorship.

Abstract

Accurate in-season crop type classification is crucial for the crop production estimation and monitoring of agricultural parcels. However, the complexity of the plant growth patterns and their spatio-temporal variability present significant challenges. While current deep learning-based methods show promise in crop type classification from single- and multi-modal time series, most existing methods rely on a single modality, such as satellite optical remote sensing data or crop rotation patterns. We propose a novel approach to fuse multimodal information into a model for improved accuracy and robustness across multiple years and countries. The approach relies on three modalities used: remote sensing time series from Sentinel-2 and Landsat 8 observations, parcel crop rotation and local crop distribution. To evaluate our approach, we release a new annotated dataset of 7.4 million agricultural parcels in France (FR) and Netherlands (NL). We associate each parcel with time-series of surface reflectance (Red and NIR) and biophysical variables (LAI, FAPAR). Additionally, we propose a new approach to automatically aggregate crop types into a hierarchical class structure for meaningful model evaluation and a novel data-augmentation technique for early-season classification. Performance of the multimodal approach was assessed at different aggregation level in the semantic domain spanning from 151 to 8 crop types or groups. It resulted in accuracy ranging from 91% to 95% for NL dataset and from 85% to 89% for FR dataset. Pre-training on a dataset improves domain adaptation between countries, allowing for cross-domain zero-shot learning, and robustness of the performances in a few-shot setting from France to Netherlands. Our proposed approach outperforms comparable methods by enabling learning methods to use the often overlooked spatio-temporal context of parcels, resulting in increased precision and generalization capacity.

Keywords: agriculture, deep learning, remote sensing, Earth Observation, Hierarchical model, Multimodal, Time series, Crop rotation, Long-Short-Term-Memory, satellite, Sentinel-2, Copernicus, Common Agriculture Policy, parcel, Crop type, Crop yield forecasting, Crop production, Classification

1. Introduction

Crop-type maps are an essential element used in crop production monitoring that feed into global food security assessments (Porter et al., 2014). Satellite Earth Observation (EO) systems offer a valuable data source for crop classification due to the synoptic, repeated, consistent, and timely availability of observations (Weiss et al., 2020). Since 2015, the data from the European Union (EU)’s Copernicus program, in particular those of the Sentinel-1 (S1) and Sentinel-2 (S2) sensors, provide systematic and consistent EO data at a spatial resolution generally higher than the size of most agricultural parcels. Over the last decade, many crop-type mapping studies and operational systems based on EO have been carried out, leveraging the abundant data available.

1.1. Related Works

The related works have been separated in three subsections: EO-based-only models, models using crop-rotations, and works

on early-season predictions. We restrain this section to Learning methods, as it is the focus of this work and as they have proven to lead to better results at large scale.

1.1.1. EO-based Models

Rußwurm et al. (2019b) classify 13 crop types at the parcel-level using all the available 13 spectral bands of Sentinel2 data from French Brittany during the 2017 growing season. They compare a Transformer-Encoder (Vaswani et al., 2017) and a Recurrent Neural Network of Long-Short-Term-Memory (LSTM) type (Hochreiter & Schmidhuber, 1997) and find that both models perform similarly, with the Transformer-Encoder and LSTM achieving both comparable accuracy and macro-F1, respectively close to 0.69 and 0.59. Rußwurm & Körner (2020) design a crop classifier at the parcel-level using S2 data from three regions of Germany and compare different approaches to model the signal, including a Transformer and an LSTM. They achieve overall accuracies between 0.85 and 0.92 using the LSTM, depending on the number of classes considered.

They conclude that data processing was useful for those kind of models. A similar approach was taken by [Rußwurm et al. \(2019c\)](#) on 40k parcels in Central Europe using S2 data, for which they proposed a new early classification mechanism to enhance a classical model with an additional stopping probability based on previously seen information. Furthermore, [Rußwurm & Körner \(2018\)](#) tackled the task of crop classification at the pixel level, by accounting for the spatial variation to detect parcels boundaries, using Convolutional Neural Network-Long-Short-Term-Memory (CNN-LSTM) on S2 images to classify 17 types of crops in a unique German region. [Sainte Fare Garnot et al. \(2019\)](#) proposed to use a Convolutional Neural Networks (CNN) before a Recurrent Neural Network (RNN) to learn the aggregation of the parcel pixels instead of classically averaging them, and applied their system on 200k parcels of the south-west of France (FR). In the end, [Sainte Fare Garnot et al. \(2020\)](#) proposed a smart method to tackle parcel-level crop classification, by randomly sampling pixels of the parcels to learn expressive descriptors that are processed by a transformer. The application of their models was carried out on 191k parcels located in the south of FR, encompassing 20 crop classes.

Finally, only some works attempt few-shot classification (i.e., learning a classifier for a new dataset given only a few examples, zero-shot when no examples are available ([Peng et al., 2018](#))) with EO-data because it has been a difficult task for a long-time, knowing that a majority of the systems work poorly without domain data. Nevertheless, [Rußwurm et al. \(2019d\)](#) and [Tseng et al. \(2021a\)](#) both propose to use the MAML meta-learning algorithm in order to tackle few-shot crop or land cover classification at the pixel-level, using EO data only. The former on the *CropHarvest* dataset from [Tseng et al. \(2021b\)](#), which is an aggregation of satellite datasets for crop type classification containing annotation at the pixel levels, without an harmonized label taxonomy between the examples of different domains. The latter on the Sen12MS ([Schmitt et al., 2019](#)) and DeepGlobe Challenge ([Demir et al., 2018](#)) datasets for land cover classification.

1.1.2. Crop-rotation-based Models

Crop rotation is an essential agronomic practice for sustainable farming and preserving long-term soil quality. A good understanding and design of crop rotation is vital for sustainability and mitigating the variability of agricultural productivity induced by climate change ([Bohan et al., 2021](#)). Crop rotation patterns are complex and non-stable in time, often dependent on farmer management decisions and subject to changes due to economic considerations and administrative regulations ([Dogliotti et al., 2003](#)). As a result, expert knowledge-based models have limitations in terms of accuracy and applicability over large areas and long periods. Alternative approaches, such as estimation of crop sequence probabilities using survey data and hidden Markov models have been demonstrated in FR ([Xiao et al., 2014](#)), but these methods are not always feasible at large scale due to the extended size of the required sample.

Past research has focused on using machine learning techniques to predict crop rotations. In [Osman et al. \(2015\)](#), a

Markov Logic model is used to predict the following year's crop in FR, achieving an accuracy of 60%. Other studies have utilized deep neural networks, such as [Yamasu et al. \(2020\)](#), which reaches a maximum accuracy of 88% on a 6-class portion of the US Cropland Data Layer (CDL) dataset over 12 years.

Only three studies ([Johnson & Mueller, 2021](#); [Giordano et al., 2020](#); [Quinton & Landrieu, 2021](#)) have been identified that combine the use of crop rotations and satellite time-series data with deep learning. [Johnson & Mueller \(2021\)](#) applied this method over several years to derive near real-time CDL. However, this methodology is constrained to a small number of crop types and the use of a Random Forest classifier, while recent advancements in deep learning have shown significant improvements in such high-data regime problems. [Giordano et al. \(2020\)](#) used Conditional Random Fields to model the temporal dynamics of crop rotations. They focused on two French regions with very different climate conditions and agricultural practices, using around 9,230 and 1,902 parcels with 2 years of data. [Quinton & Landrieu \(2021\)](#) propose to use a Pixel-Set Encoder with a Lightweight Temporal Attention Encoder (PSE-LTAE) ([Sainte Fare Garnot et al., 2020](#)) combined with a multi-year classification method. They represent the past crops with a one-hot encoder that they sum, without modeling the dynamics of the sequence. In our work, we not only focus on modeling the sequential aspects of crop rotations, but also incorporate the Remote Sensing (RS) signals from previous years.

1.1.3. Early Season Classification

While end-of-season crop type maps have a great interest for agricultural land monitoring ([Weiss et al., 2020](#)), in-season crop production monitoring requires a more rapid response, including before-harvest crop type map releases. Some works have also focused on tackling early-season classification. [Rußwurm et al. \(2019a,c\)](#) proposed to solve the problem in an elegant way, with an adapted cost function that only rewards the classifier for an early classification if the right class has been predicted with a respectable degree of accuracy. They extend this work in [Rußwurm et al. \(2023\)](#) by presenting end-to-end Learned Early Classification of Time Series, also classifying crops at the parcel-level in FR, Germany, Ghana and South Sudan.

Without using a special cost function, [Weilandt et al. \(2023\)](#) use a PSE-LTAE, a technique initially proposed by [Barriere & Claverie \(2022\)](#), on hierarchical LSTM for crop-type classification at the parcel-level. They perform data-augmentation by randomly cropping the end of the EO time series during training. The data-augmentation technique boost the performances of early-season classification. They also compared separate models trained on data cropped up to a unique certain period in the year (i.e. one model for one period), which is not efficient in terms of computation and yielded similar results.

1.2. Positioning and Objectives

To the best of the authors' knowledge, there are some gaps in the existing literature.

A significant amount of research has focused on using remote sensing to predict crop types at the pixel or parcel level using

only EO and in-situ observations of the current year, treating the signal as independent from one year to another. Other studies have used crop rotations of parcels to address pre-season prediction of crop types (Osman et al., 2015; Yaramasu et al., 2020), but the lack of sufficient information in the signal (i.e. short length of the time series) limits their performance even when targeting on minor classes. While the integration of RS data with crop rotations has been investigated in certain studies (Giordano et al., 2020; Quinton & Landrieu, 2021), no one has yet taken this analysis a step further by incorporating its dynamic modeling.

The dataset we have released to support our development is significantly larger than the similar one introduced above (Quinton & Landrieu, 2021). We have collected data for a minimum of 5 years and have gathered information on approximately 6.8 million (in FR) and 600 thousand parcels (in the Netherlands (NL)), which is more than three orders of magnitude greater than the typical dataset size used in other studies. Because of its diversity, we propose a method to aggregate the crops at the regional-level.

The contributions of this study are 5-fold:

- (i) We release a new dataset of more than 7.4 million parcels with their associated crops, and RS signals for the last five years in FR and NL. This allows the integration of crop rotation patterns with the remote sensing signal.
- (ii) We create a dataset-agnostic technique to automatically group crops together, leveraging expert knowledge from the EuroCrops (Schneider et al., 2021) taxonomy and derive local crop distribution. This new method allows us to detect the principal crop types from any dataset and to group them in a meaningful way.
- (iii) We construct a novel approach for crop type mapping from crop rotations and Sentinel-2 optical time series in a multimodal way using a hierarchical LSTM network. This approach is unique in its conception as it fuses large amounts of temporally fine-grained EO data with crop rotation analysis in an advanced deep learning method. The crop rotations and the S2 time series are enhanced by previous-year crop distributions of the neighbouring parcels.
- (iv) We develop a data-augmentation technique for the in-season classification, by randomly cropping the end of the RS time-series data. This allows our model to classify parcels before the end of the season, a crucial feature for real-life application of crop monitoring.
- (v) We assess the cross-domain generalization potential of the framework based on a modified nomenclature of EuroCrops.

2. Materials

This section presents a description of the study area and the EO data processing procedure.

2.1. Crop reference data, study area, and harmonization of parcel data

The Geospatial Aid Application (GSA) corresponds to the annual crop declarations made by EU farmers for Common Agricultural Policy (CAP) area-aid support measures. The electronic GSA records include a spatial delineation of the parcels. A GSA element is always a polygon of an agricultural parcel with one crop (or a single crop group with the same payment eligibility). The GSA is operated at the region or country level in the EU 27 member states, resulting in about 60 different designs and implementation schemes over the EU. Since these infrastructures are set up in each region, data are not interoperable at the moment, and the legends are not semantically harmonised. Furthermore, only few EU member states release GSA data as open data, although the overall trend is towards increasingly opening up the data for public use.

Some efforts have been made to provide harmonised GSA dataset over the EU. AI4boundaries (d’Andrimont et al., 2023) provides harmonized parcel geometries over 7 countries in the EU to benchmark method for parcel delineation. EuroCrops (Schneider et al., 2021) proposed a semantic harmonisation framework to harmonise the legend of GSA across different countries. This harmonisation is open source and is maintained by the community¹. While EuroCrops provides a unique effort so far, this work is still in progress especially with regards to the time dimension. A recent European Commission Implementing Regulation (EU) 2023/138² identifies a list of specific high-value datasets and the arrangements for their publication. This should be a game changer in the opening of the GSA for public access in the future and thus foster their use for research.

For this study, FR and the NL were selected because of i) their open parcel data availability, ii) their EU representativeness in covering a latitude range from 40° to 55° Northern latitude as well as four biogeographic regions (i.e. Atlantic, Continental, Alpine and Mediterranean) and iii) the countries have different size and landscape. Parcel GSA data from 2015 to 2021 over FR and from 2009 to 2021 over the NL were collected (Table 1).

2.2. Geometric minimum common parcel extraction through time

GSA are delivered yearly as a set of polygons outlining agricultural parcels. From year-to-year, the parcel boundary may change. We intersected GSA data (i.e. 2013-2020 for NL and 2015-2020 for FR) in order to extract minimum common area, each with a distinct multi-annual crop sequence, named hereafter Feature Of Interest (FOI). Since FOI are the cross-section of varying parcel bounds, their overall size is smaller than the annual GSA parcels. We discarded any FOI with an area of less than 0.1 ha and 0.5 ha for NL and FR, respectively. The total FOI area cover 85% and 93% of the average GSA area for NL and FR respectively (the “stack” entries in Table 1). For each FOI, a crop type sequence was extracted, as well as the remote sensing time series (Fig. 1).

¹<https://github.com/maja601/EuroCrops>

²https://eur-lex.europa.eu/eli/reg_impl/2023/138

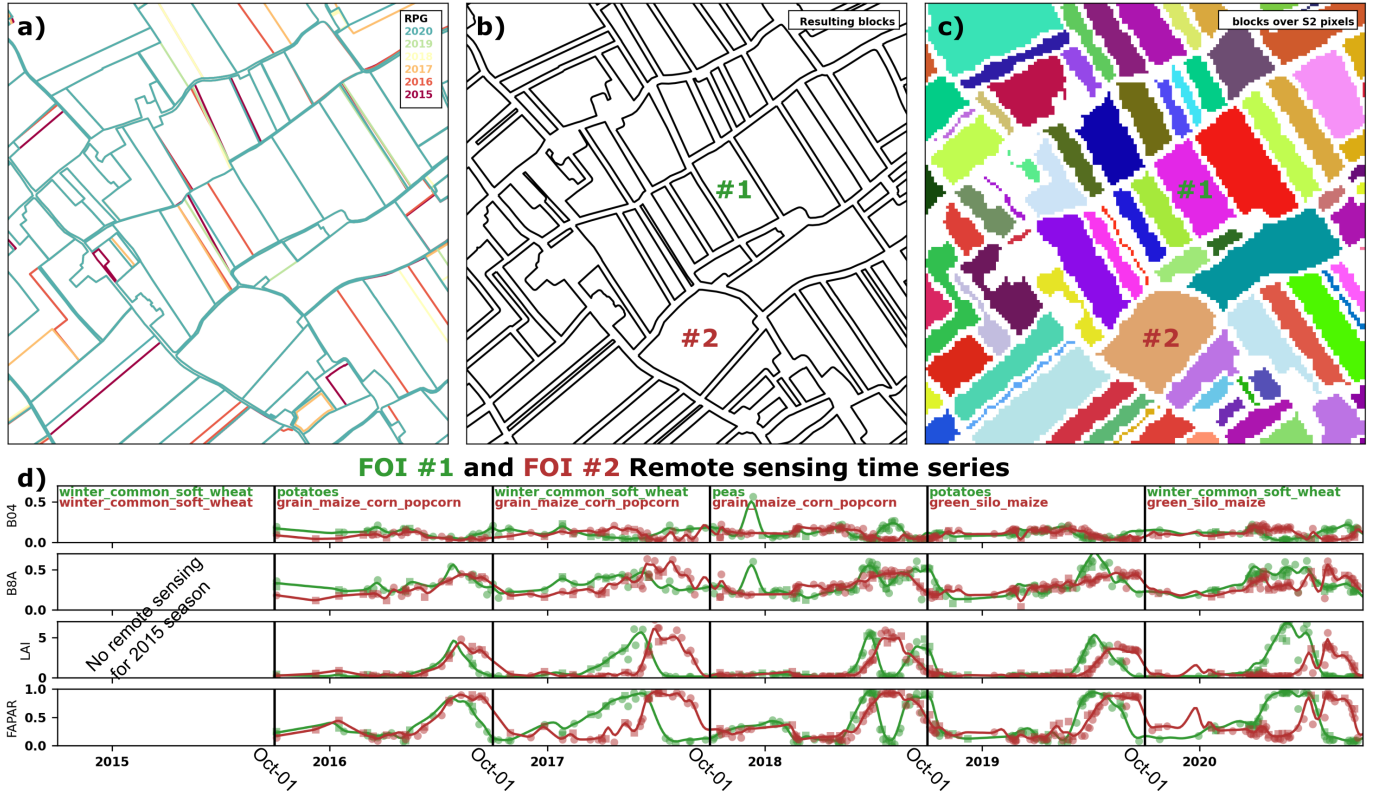


Fig. 1: Feature Of Interest (FOI) extraction, time series extraction and smoothing. a) the map shows an overlap of the six GSA layers; b) Resulting blocks corresponding to the intersection of the six GSA layers, reduced by an inner buffer; c) rasterized version of the blocks used for extracting the S2 data; d) full S2 and crop types time series of two selected FOI (shown in panels a-c). Yearly crop types are displayed on the top sub-panel. Input variables time series are displayed using daily observations (circles and squares correspond to S2 and Landsat 8 (L8) data, respectively) and smoothed signal (used as LSTM inputs).

Table 1: Original Geospatial Aid Application (GSA) parcel numbers and area per year used in the study for France (FR) and Netherlands (NL). The number of distinct crop types are provided using original GSA and aggregated using EuroCrops. The "stack" lines correspond to the Feature Of Interest (FOI, see section 2.2).

Country	Year	RS	# distinct crop types original	# distinct crop types aggregated	Number of polygons	Total area (1000 ha)
NL	2013	✗	76	41	762,725	1,855
NL	2014	✗	75	41	765,006	1,859
NL	2015	✗	260	117	790,930	1,873
NL	2016	✓	296	133	786,572	1,871
NL	2017	✓	300	136	785,710	1,882
NL	2018	✓	312	135	774,822	1,871
NL	2019	✓	317	139	772,565	1,868
NL	2020	✓	326	141	767,034	1,872
NL	stack		401	148	596,762	1,407
FR	2015	✗	261	150	9,434,672	27,856
FR	2016	✓	261	147	9,334,043	27,876
FR	2017	✓	280	148	9,393,747	27,889
FR	2018	✓	282	149	9,517,878	27,917
FR	2019	✓	241	149	9,604,463	27,960
FR	2020	✓	239	148	9,778,397	27,998
FR	stack		319	151	7,051,683	25,495

2.3. Earth Observation processing

Remote sensing data were extracted from S2 MSI and L8 OLI sensors. While the GSA data spans from 2013 and 2015, for NL³ and FR respectively, the remote sensing data were used starting 2016 cropping season (i.e., from October-2015), corresponding to the first cropping season with both sensors in-orbit.

S2 MSI products with Level-2A surface reflectance data were downloaded from the Copernicus Open Access Hub. L8 OLI surface reflectance data were downloaded from the L30 products of the Harmonized Landsat Sentinel-2 (HLS) data set. For both products, L2A and L30 Quality Assessment (QA) layers were used to mask non-surface-related information. We masked all pixels flagged as cloud, cloud-shadow, cirrus and snow.

Leaf Area Index (LAI) and Fraction of Absorbed Photosynthetically Active Radiation (FAPAR) Biophysical variables (BV) maps were derived from the S2 L2A (20m spatial resolution) and L8 L30 (30m spatial resolution) products, using the BV-NET algorithm developed by Weiss & Baret (1999). It aims to retrieve the two BV from multispectral reflectance using the inversion of the radiative transfer model PROSAIL and a back-propagation Artificial Neural Network (ANN). Following the configuration of Delloye et al. (2018), the architecture of the ANN consists of two layers: (i) one layer with five tangent sigmoid transfer functions neurons and (ii) one layer with one linear transfer functions neuron. This configuration allows for

³It starts from 2009 but we only took data from 2013

greater dynamics in the output variables (Claverie et al., 2013). The HLS products are normalised using the Bidirectional Reflection Distribution Function (BRDF) with a nadir view zenith angle and a variable sun angle (Claverie et al., 2018), while the S2 L2A products are unadjusted with BRDF. We retained these data specifications and configured two BV-NET models to account for them. For both product types, the cosine of the solar zenith angle was included in the BV-NET input set; for S2 L2A, the view zenith and relative azimuth angles were also included.

Only the Red and Near Infrared bands (NIR) were kept for further analysis; the remaining spectral bands were discarded. Four variables (LAI, FAPAR, Red band and NIR band) pixel-based maps were thus used to derive time series per FOI. Pixels whose centres fell within the FOI boundaries, reduced by a 15 m inner buffer, were averaged using a zonal statistics technique; flagged values (cloud, cloud shadow, cirrus or snow) from QA layers were not included in the averaging. FOI values were only considered valid if more than 75% of the LAI pixels were valid.

Despite filtering the data using relevant QA layers, the resulting FOI-based time series are still contaminated by missed cloud, cloud shadow, haze or dense atmosphere. To remove these remaining outliers, we applied a Hampel filter using red and NIR bands to discard cloud and cloud-shadow in the time series respectively; the parameters of the filter follow Claverie et al. (2018).

Finally, filtered time series of four variables aggregated at FOI level were smoothed individually using a Whittaker filter.⁴ The time series are first gap-filled in time using a linear interpolation and a time step of 2 days. We applied the Whittaker configuration with V-curve optimization of the smoothing parameter and expectile smoothing using asymmetric weight, with an "Envelope" value of 0.9 and a tested lambda range between -1 and 1 (Eilers et al., 2017). This results in a smoothed time series with a time step of 4 days and no interruption between the seasons.

3. Methods

The features extraction and the model architecture are first described in section 3.1), followed by a description of the learning model and the integration of features as observations (section 3.2). In Section 3.3, we delve into the early-season data augmentation technique. Then in Section 3.4, we explore the training process and the application of models in various countries. Finally, section 3.6 outlines the processing facilities utilized in the study and includes links to the data and code.

3.1. Models description

A series of models were developed involving various configuration and input modalities. The three modalities are RS, Crop Rotation (CR) and Crop Distribution (CD) (see the conceptual framework in Fig. 2). This section describes the model and the

integration of the data as features. All the models presented in this section are summarized in Table 2.

Crop rotations have been modeled in a manner similar to how words are structured within a language model (Mikolov et al., 2010). This modeling process is further enhanced by adding S2 time-series data, which is treated as analogous to the prosody of a speaker (Schuller et al., 2016), i.e. the pattern of intonation, stress and rhythm in a speech. Ultimately, the high-level spatial crop distribution features we add on the last layer of the network can be seen as the distribution of the words generally used by the speaker.

3.1.1. Features extraction

Crop Rotation

For each parcel, we extracted the crop sequence which corresponds to the CR feature.

Remote Sensing temporal integration

We integrated the RS time series into features using a sliding window of size W months with a step of size $s_w = 0.5W$, obtaining a sequence of $t_w = \frac{12}{s_w}$ inputs windows for 12 months. On every time window, each signal was integrated using statistical functionals following an approach commonly used for speech data (Schuller et al., 2016). For each window, we used a set of F statistical functionals to represent the signal as a fixed vector.

Crop Distribution

For each FOI, we computed the area of each crops in a circle of radius r and turned it to percentage of the total cropped area. The rationale to use spatial crop type distribution around the parcel is that, at the scale of a country, agricultural practices vary geographically due to the type of soil and its suitability for crop production, local agro-meteorological conditions, economic and historical factors. In the absence of major shocks, the distribution of the crop types in a region is expected to be stable over the years (Merlos & Hijmans, 2020), which determines the *a priori* probability of local crop occurrence. We integrate this local information by adding a vector representing the CD over the surrounding crop types centered around each parcel.

3.1.2. Architecture of the models

Baselines using Year-Independent models

We used two baselines models that treat the RS time series signal in a classical way without using hierarchical networks and without modeling the dynamics between the years. One unimodal model is using only RS data and another one is multimodal using RS and CR. **These models are referred to as IntraYE_{RS} and IntraYE_{MM}, respectively.**

As stated in Rußwurm et al. (2019b), they only consider the time series of a single year, without incorporating a multi-year modeling approach for the RS data which is a key aspect of our proposed approach. This unimodal network is the identical component utilized for encoding the RS signal at the year-level (one green Intra-Year Encoder (IntraYE) in Fig. 3). This provides a strong RS unimodal baseline. The second baseline that

⁴as developed by <https://github.com/WFP-VAM/vam.whittaker>

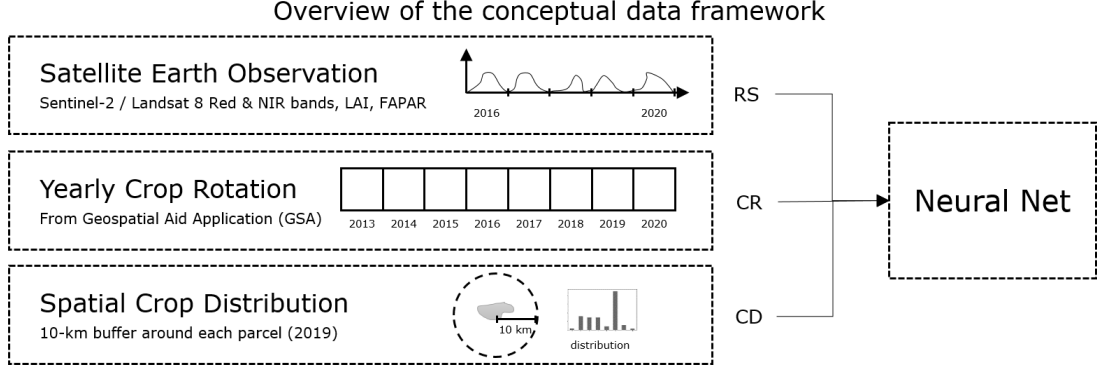


Fig. 2: Overview of the conceptual data framework for crop classification to leverage satellite optical time series, yearly crop rotation history, and spatial local crop distributions.

Table 2: Summary of the different models used in this paper, using Crop Rotations (CR), Remote Sensing (RS), and Crop Distribution (CD).

Models	CR	RS	CD	Modelisation-level		Hierarchical
				Within year	Between years	
IntraYE _{RS}	✗	✓	✗	✓	✗	✗
IntraYE _{MM}	✓	✓	✗	✓	✗	✗
InterYE _{Crop}	✓	✗	✗	✗	✓	✗
InterYE _{RS}	✗	✓	✗	✗	✓	✗
InterYE _{MM}	✓	✓	✗	✗	✓	✗
HierE _{RS}	✗	✓	✗	✓	✓	✓
HierE _{MM}	✓	✓	✗	✓	✓	✓
HierE _{final}	✓	✓	✓	✓	✓	✓

we add comes from the work of [Quinton & Landrieu \(2021\)](#), which integrates the CR modality by using a one-hot encoder vector of the past crop sequence. In our case, as we see the crops as words, this would mean a simple Bag-of-Words ([Harris, 1954](#)), hence we will call it Bag-of-Crops (BoC). Although this type of representation is known not to work well for short texts like tweets or speech turns ([Benamara et al., 2016](#); [Barriere et al., 2018](#); [Barriere, 2017](#); [Barriere et al., 2017](#)), we can expect better results with crop sequences which are considerably less complex than natural language.

Multi-year non-hierarchical models

Following the introduction, a set of novel model architectures is suggested hereafter, and their performance is evaluated in comparison to the existing baseline models. We first aimed to model the sequence of years with a recurrent encoder. These models use year-level features and are called Inter-Year Encoder (InterYE). This corresponds to the orange top Encoder in [Fig. 3](#), modeling the sequence of years.

We modeled the multi-annual crop rotations in a language model fashion by representing the crops as tokens and learning to predict the next one. This model takes the past sequence of crops (c_1, \dots, c_t) as inputs and output the new crop c_{t+1} , modeling the crop rotation dynamics through the years. This corresponds to the orange InterYE in [Fig. 3](#), if only using crop embeddings. It does not use the blue local crop distribution vector. **This unimodal model is denoted InterYE_{Crop}**, corresponding to a unimodal Crop Rotations model.

Using solely previous rotations to forecast future crop yields

results in inadequate performance due to the limited amount of information provided. Therefore, we decided to enhance the model’s robustness by incorporating satellite data, leveraging either the consensus principle or the complementary principle ([Xu et al., 2013](#)). We enhanced the unimodal model InterYE_{Crop} by adding year-level information from RS. This corresponds to the orange InterYE in [Fig. 3](#), with a green vector being the year-level concatenation of the RS signal (without being processed by the green IntraYE). It does not include the blue local crop distribution vector. **This model is denoted as InterYE_{MM}**, corresponding to a non-hierarchical multimodal model with RS. If the model only uses the RS modality, then it is denoted as InterYE_{RS}.

Multi-year hierarchical models

We chose to model jointly the inter-year and intra-year dynamics with a hierarchical model composed of one network modeling the RS dynamics within a year underneath another network modeling the rotation dynamics between the years. We processed the RS signal beforehand using another RNN, before concatenating this unimodal RS vector obtained with the crop embedding, in a hierarchical way. This corresponds to the orange color top InterYE and the green color IntraYE in [Fig. 3](#), modeling between the years as well as within a year.

We incorporated the sequential aspect of the RS time-series by processing the RS features at the year level with a first sequential encoder before adding their yearly representation into the second neural network modeling the crop types, leading to a hierarchical network ([Serban et al., 2015](#)). This corresponds to

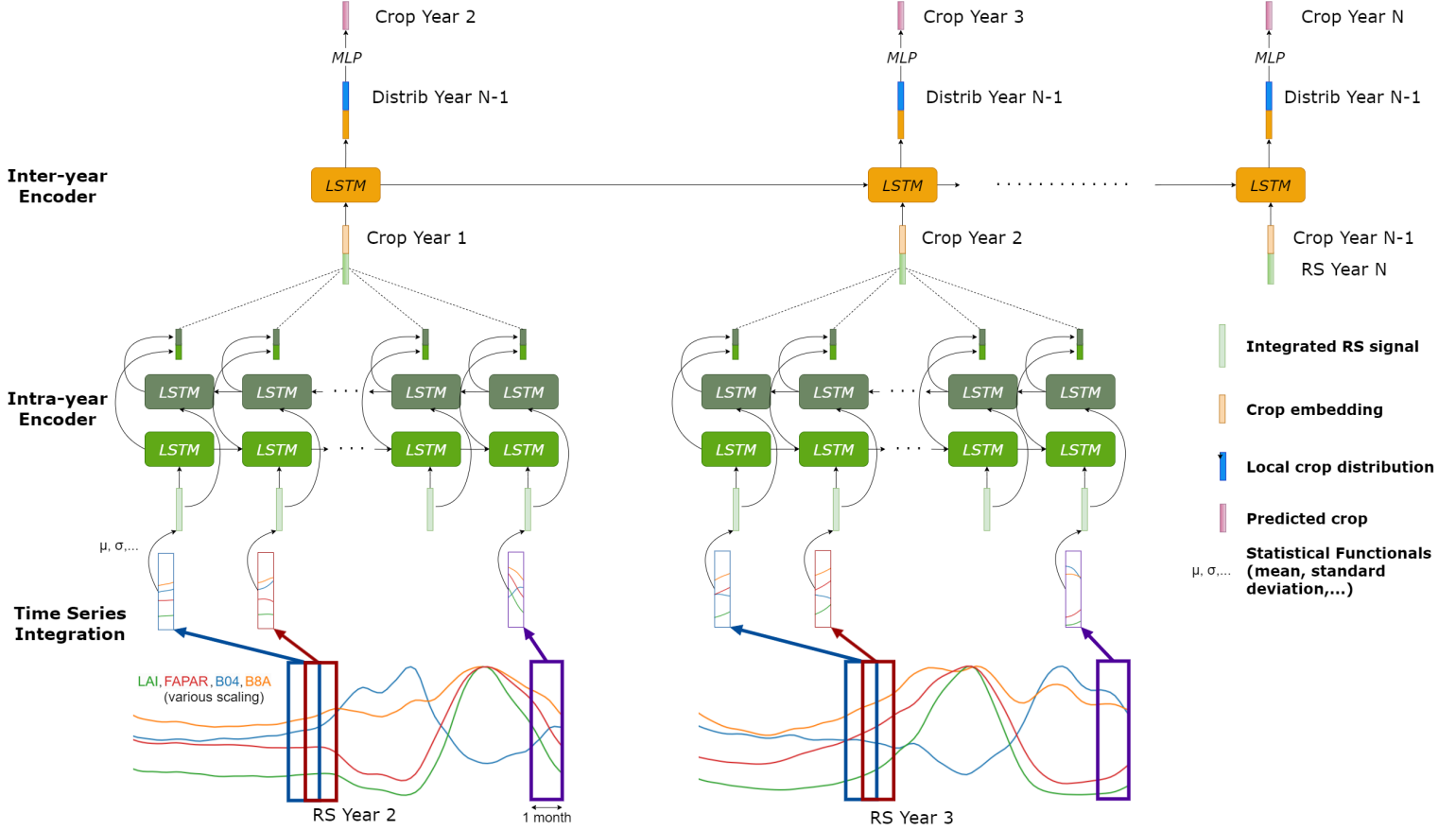


Fig. 3: Hierarchical Multimodal Model Conceptual Diagram.

the orange Inter-year Encoder in Fig. 3, processing the crop embeddings and the RS embeddings coming from the green IntraYE. It does not use the blue local crop distribution vector. **This model is denoted as HierE_{MM}**, corresponding thus to a hierarchical iIntraYE and InterYE to model both crop rotation and RS time-series.

We enhanced the model by adding the CD vector after the IntraYE because it is a high-level feature regarding the task we are tackling and the deeper you go into the layers the higher-level the representations are w.r.t. the task (Sanh et al., 2018). This corresponds to the full network presented in Fig. 3, including the blue local crop distribution vector. **This model is denoted as HierE_{final}**, corresponding thus to a hierarchical IntraYE and InterYE to model the three modalities.

3.2. Automatic Hierarchical Label Aggregation

3.2.1. Rationale

Training and evaluating a model at large scale, on regions that contain different agro-climatic zones is complex due to the heterogeneity of the temporal and spectral representations of the crops and variability of the climate and agricultural practices. Indeed, if the labels distribution is highly variable between two datasets, one label that was representative of one domain would become not representative in the other. In this work we propose an aggregation of the labels, that would be on the one hand representative of the dataset, and on the other

hand thematically pertinent. In this way, it should be possible to evaluate the performances of the classification model at different scales: using all the labels from the region, even the ones with very few examples, then using an aggregation of labels that is representative of the region. This also offers the advantage to evaluate a model on two different datasets with a relevant evaluation on each dataset.

3.2.2. EuroCrops

The Hierarchical Crop and Agriculture Taxonomy version 2 (HCATv2) from EuroCrops offers a knowledge graph regrouping crops together in a hierarchical way that is coherent with agricultural practices. It contains 393 classes, which are defined at six hierarchical levels of which the first two are fixed due to compatibility with other taxonomies. For example 33-01-01-05-01 corresponds to the class *Summer Oats*, which is included in its parent class 33-01-01-05-00 (*Oats*) and its grand-parent class 33-01-01-00-00 (*Cereals*). Nevertheless, it is not possible to merge the labels only using the hierarchy because some branches go to a deeper level than others. For example, the class *Capsicum* is level-4 and represent 0.004% of FR, which is the same level than the class *Cereal* representing 32%. HCATv2 (Schneider et al., 2021) was used to represent a Sankey diagram linking the French GSA (left) and the Dutch GSA (right), using HCATv2 (Schneider et al., 2021, centre) is represented in Fig. A.1 using 40 main crop types for

each country⁵.

3.2.3. A Dataset-Agnostic Method to Generate Labels

EC labels have heterogeneous distribution and level of interest because of geographically constrained occurrence. We propose a method to merge non-representative crops together to only keep the most relevant. The method is applied for the evaluation only. By using a dataset-agnostic algorithm, we take the best of both worlds by fusing expert knowledge and data-driven method. The method is applicable at any geographic scale and fully automatic.

We create a graph using EuroCrops and the distribution of each crops in the dataset. The crops are merged together, with the other sibling crops in the EuroCrops graph using their parent-class, and so-on. Each node n_{ijkl} is a class, with the number of FOI being its weight w_{ijkl} . Each class is link with its parent-class n_{ijk} . At the beginning, each weights are initialized to zero, except the ones of the end nodes.

With $i, j, k, l \in \mathbb{N}^4$ being the indices of the nodes in the 4 levels of hierarchy, for each node n_{ijkl} starting by deepest level l : if its weight w_{ijkl} is above a threshold of representativeness th then it becomes a class of interest, otherwise w_{ijkl} is transferred to the weight w_{ijk} of its parent-class n_{ijk} . When all the child nodes of n_{ijk} have been seen, pass to the next node $n_{ijk'}$.

3.3. Early-Season data augmentation

The end-of-season models that are trained with the data from the whole season are known not suited to classify at early-season. We propose a data-augmentation technique in order to help the model to classify a sample even without getting the whole time series of the season. We follow the approach of Barriere & Claverie (2022) by randomly cropping the end of the vector feature of the RS data $RS = (RS_1, \dots, RS_{t_w})$. To proceed, we sampled an integer $t < t_w$ (the maximum length of the time series) from a discrete probability distribution \mathcal{D} , and used this number to crop the remote sensing data, as if it was ending before:

$$RS_{cropped} = RS[:t] = (RS_1, \dots, RS_t), \quad t \sim \mathcal{D}$$

3.4. Transfer learning between countries

We ran several experiments in order to take advantage of the normalized taxonomy that we used for both countries, by investigating the potential of transferring knowledge between different domains. For these purposes, we compared the performances of a model trained from scratch (i.e. Vanilla) and a model pre-trained over a country before being fine-tuned over another one. This pre-training allows to transfer knowledge from a source task and domain to a target task and domain. We tested this approach in zero-shot and few-shot settings. For the few-shot, we selected 2^N (with $N \in \{4, 6, 8, 10\}$) examples of every aggregated class (see Section 3.2), in a random way. We

added more and more data increasingly so that all the examples from 2^{n_1} are comprised in 2^{n_2} , with $n_1 < n_2$. A summary of the different experiments can be seen in Table 3.

3.5. Implementation

RS features

For each FOI and each year, the RS time series of the four variables are integrated, using a sliding window of size $W = 1$ month; this leads to $t_w = 24$ sliding windows. By utilizing this setup, we obtain some overlap between the windows, which should prevent loss of information by breaking the signal dynamics, albeit with a slight trade-off of redundancy in the features. The $F = 7$ statistical functional used were: average mean, standard deviation, min, max, median, first quartile, third quartile. As a total, we obtained $4 \times 24 \times 7 = 672$ features per FOI per year.

Encoders

We compared several type of models using different architectures and different modalities. Because our work mainly focuses on how to integrate multimodal data, we opted to use Recurrent Neural Network-Long-Short-Term-Memory (RNN-LSTM) backbones, proven competitive for this kind of task (Rußwurm & Körner, 2020). Our method is also applicable using other encoders such as transformers (Vaswani et al., 2017) or Gated Recurrent Units (Chung et al., 2015).

The Inter-year encoder, we first add an embedding layer to transform the crop type c_t at year t into a vector $\mathbf{emb}_t = f_e(c_t)$. This embedding vector \mathbf{emb}_t is used as input of the LSTM to produce a hidden state h_t at year t as seen in Equation 1, which will be used to predict the next crop c_{t+1} in Equation 2.

$$\mathbf{h}_t = \text{LSTM}_y(\mathbf{emb}_t, \mathbf{h}_{t-1}) \quad (1)$$

$$P(c_{t+1}|c_t, \dots, c_1) = f_c(\mathbf{h}_t) \quad (2)$$

The RS features were integrated at the year-level into a feature vector \mathbf{RS}_t before the modeling of the crop types by the LSTM. We feed the year t feature vector \mathbf{RS}_t into a neural network layer f_{rs} to reduce its size and then concatenate it with the crop embeddings before the LSTM (see Equation 3), using \mathbf{emb}_{MM_t} instead of \mathbf{emb}_t in Equation 1.

$$\mathbf{emb}_{MM_t} = [\mathbf{emb}_t, f_{rs}(\mathbf{RS}_t)] \quad (3)$$

For the IntraYE, we chose to use a bidirectional LSTM (biLSTM) with a self-attention mechanism (Bahdanau et al., 2016) following the assumption that some parts of the year are more important than others to discriminate the crop type. The biLSTM is composed of two LSTM, one of which reads the sequence forward and the other reads it backward. The final hidden states are a concatenation of the forward and backward hidden states. For a sequence of inputs $[\mathbf{RS}_{t_1}, \dots, \mathbf{RS}_{t_w}]$ it outputs w hidden states $[\mathbf{h}_{RS_{t_1}}, \dots, \mathbf{h}_{RS_{t_w}}]$. The attention layer will

⁵An interactive version of the diagram without class limitation is available on https://jeodpp.jrc.ec.europa.eu/ftp/jrc-opendata/DRL/CropDeepTrans/data/sankey_All_crops.html.

Table 3: Transfer learning summary. $N \in \{4, 6, 8, 10\}$ for the few-shot experiments.

Name	Pre-Training	Training	Testing	# data from target	Models
few-shot-NL	\emptyset	NL	NL	2^N	HierE _{final}
few-shot-FR	\emptyset	FR	FR	2^N	HierE _{final}
Vanilla-FR	\emptyset	FR	FR	100%	All models
Vanilla-NL	\emptyset	NL	NL	100%	All models
0-shot-NL	\emptyset	FR	NL	0	HierE _{final}
Transfer-few-shot-NL	FR	NL	NL	2^N	HierE _{final}
transfer-NL	FR	NL	NL	100%	HierE _{final}
Transfer-FR	NL	FR	FR	100%	HierE _{final}

compute the scalar weights u_{t_w} for each of the $\mathbf{h}_{RS_{t_w}}$ (see Equation 4) in order to aggregate them to obtain the final state \mathbf{h}_{RS_t} (see Equation 5).

$$u_{t_w} = \text{att}(\mathbf{h}_{RS_{t_w}}) \quad (4)$$

$$\mathbf{h}_{RS_t} = \sum_w u_{t_w} \mathbf{h}_{RS_{t_w}} \quad (5)$$

For the crop distribution, we concatenated the hidden state \mathbf{h}_t of the LSTM with the crop distribution vector \mathbf{d} and mixed them using two fully connected layers f_{fc1} and f_{fc2} (see Equation 6). Hence, we obtain \mathbf{h}_d instead of \mathbf{h}_t before the final fully connected layer f_{fc} from Equation 2.

$$\mathbf{h}_d = f_{fc2}(f_{fc1}([\mathbf{h}_t, \mathbf{d}])) \quad (6)$$

In-country Early-season experiments

For the early-season experiments, we reduce the size of the time-series by sampling its maximum length from a discrete uniform distribution between 10 and 24: $\mathcal{D} = \mathcal{U}(10, 24)$. By setting the minimum number of steps to 10, we ensure that each sample contains sufficient information (at least 5 months) to facilitate the training phase. Knowing the start of the time-series is October, it means we do not crop the end of the time series up to 1st of March. We used the same cropping size t for all the samples of the same mini-batch.

Zero-shot, Few-shot and Cross-country Experiments

In order to investigate the potential of transferring knowledge between two different domains, we pre-trained a network on one country, before fine-tuning it over another country. For this, we simply initialized the network weights with the ones of a model already trained on the other domain. We did not freeze any layer during the fine-tuning.

For the zero-shot setting, we used a network that was trained over one country on the other country, without fine-tuning it. For the few-shot setting, we fine-tuned the network only on a subset of the target dataset, taking few examples representative of this dataset. We generated the few-shot subsets by randomly sampling 2^N of each of the aggregated class (see Section 4.1). For this, we sampled using the crop of the 2019 distribution, which was used as validation year. We think that this setup is realistic as we only sample from the aggregated classes that

are the prominent ones in each of the datasets, and the ones to calculate the metrics to validate the models.

Technicalities

We trained all the networks via mini-batch stochastic gradient descent using the Adam optimizer (Kingma & Ba, 2014) with a learning rate of 10^{-3} and a cross-entropy loss function. The number of neurons for the crop embedding layer, both the RNN internal layers, and the fully connected RS layer f_{rs} as well as the number of stacked LSTM were chosen using hyperparameters search. The sizes of the layers f_{c1} and f_{c2} are the same as the one from the second RNN state \mathbf{h}_t .

We trained our networks as for a sequence classification task, always with several years of data. The labels up to 2018 were used as training set, while the labels from 2019 were used as validation set and the labels from 2020 as test set. All results presented hereafter refer to the analysis of 2020 crop types, which are based on models trained with the period 2013-2019 for NL and 2015-2019 for FR, thus independent from the 2020 crop types observations. We zero-padded when no RS data was available (before 2016).

3.6. Processing facility, data and code

The EO extraction and processing, the classification and the benchmarking were performed on the JRC Big Data Analytics Platform (BDAP) using an HTCondor environment (Soille et al., 2018). The platform⁶ has been built upon the near-data processing concept, which prescribes placing the computing facility close to the storage units to avoid the bottleneck of delaying or degrading interconnection. Experiments with the neural networks were run using PyTorch 1.4.0 (Paszke et al., 2019) on a GPU Nvidia RTX-8000 using CUDA 12.0. The training phase allows to process between roughly 5k and 30k examples per seconds, with each example containing 4 years of data.

The data extracted and used for this study are openly available on the public FTP⁷. The code for the data processing, the labels aggregation, and deep learning experiments will be freely available after publication.⁸

⁶<https://jeodpp.jrc.ec.europa.eu/bdap/>

⁷The data can be downloaded on <https://jeodpp.jrc.ec.europa.eu/ftp/jrc-opendata/DRLL/CropDeepTrans/>.

⁸Add URL after publication

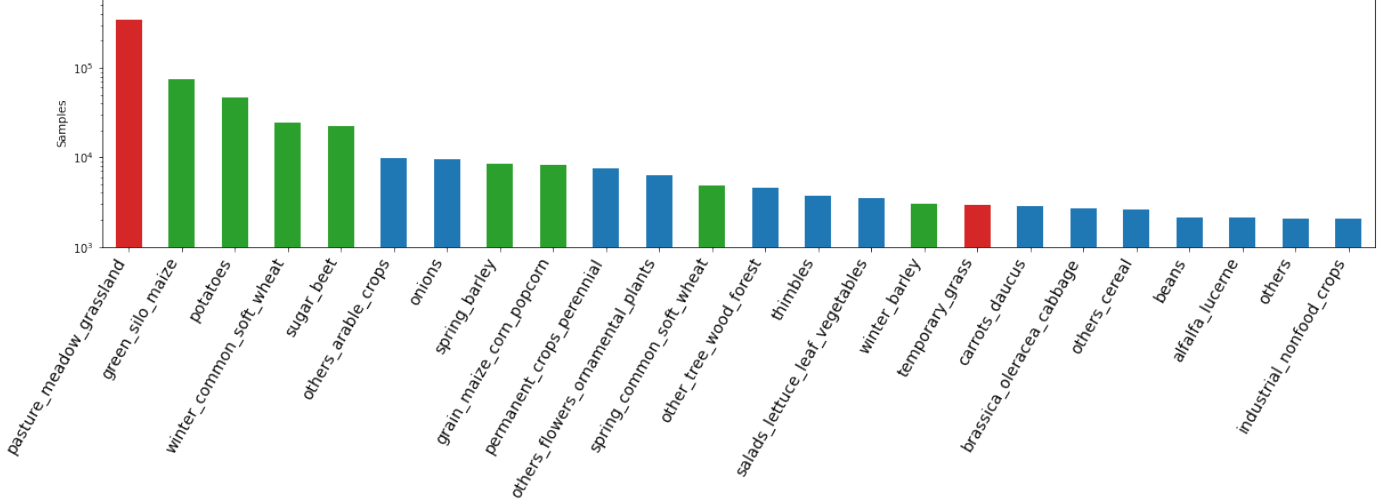


Fig. 4: Distributions of the crop types in the NL dataset for the test year (2020), after aggregation. Green bars are the selected crops for the 8-class evaluation; Red bars refer to the grasslands, and blue bars to the remaining crops.

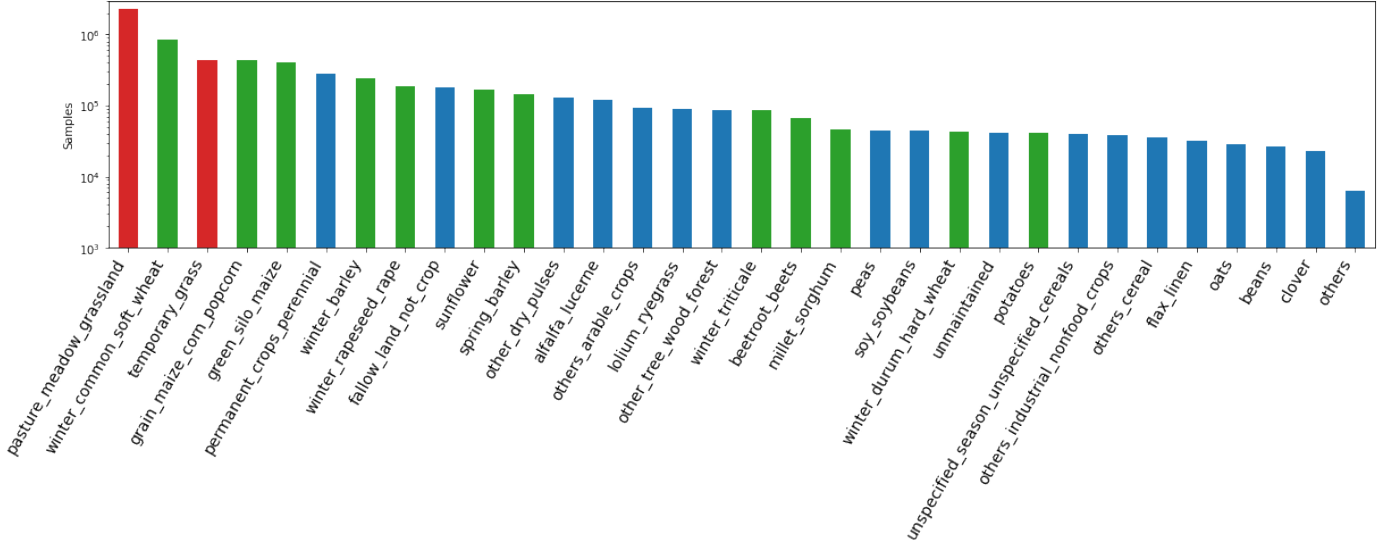


Fig. 5: Distributions of the crop types in the France dataset for the test year (2020), after aggregation. Green bars are the selected crops for the 12-class evaluation; Red bars refer to the grasslands, and blue bars to the remaining crops.

4. Experiments and Results

4.1. Feature Extractions and Label Aggregation

Crop Types

The crop types labels were extracted from the respective GSA and remapped using EuroCrops. This yields to a total of $V_{NL} = 141$ and $V_{FR} = 151$ classes, for NL and FR respectively, corresponding to $V = 225$ unique classes. We modeled the crop by a one-hot vector of size V and used it as an input to an embedding layer. The sizes of the different vocabularies determines the sizes of the respective Bag-of-Crops vectors.

The crop label categories for the 2020 test set correspond to a long-tailed class distributions, as shown for the 32-class and 24-class aggregations for the French and the Dutch data sets in Fig. 5 and Fig. 4, respectively. The models are finally validated

on a set of crops of interest from the 32-class and 24-class aggregation. Those 12 and 8 respectively for FR and the NL were selected by an expert from Food Security and identified as essential. They are shown in Fig. 5 and Fig. 4.

RS-based Features

First, the RS data retrieved as described in 2.3 were obtained. The final dataset which consists in the full time series of more than 7M FOI, for a total of more than 35M FOI-year (NL : 5 years x 596k FOI; FR: 5 years x 6.49M) are available for download, as well as the extracted features used in the experiments⁹.

⁹<https://jeodpp.jrc.ec.europa.eu/ftp/jrc-opendata/DRL/CropDeepTrans/>

Spatial Crop Distribution

The spatial CD was derived for the 2019 validation set year, i.e. not for the test year 2020. We used $r=10\text{km}$ as the radius of the circle. We rounded the probability at 10^{-4} , leading to some values being 0 when not null. We harmonized the crop list of the two datasets (FR and NL) by gap-filling the missing classes with a value of zero.

Hierarchical Label Aggregation

For each country, we set the threshold th at 0.3% of the dataset size, which roughly corresponds to 2k samples for the NL and 20k samples for FR. We classified the class *Permanent Crops* as one in both cases, as they are the simplest examples to classify when considering rotations. This was done to mitigate its impact by creating multiple labels for permanent crops. The automatic aggregation over FR and NL is shown in Fig. 6.

Dataset Segmentation and Validation

In this work, we are interested to apply early-season setting and therefore segmenting the train and test sets temporally. This provides two key advantages: we are in a real-life setting without in-situ data from the test year, and prohibit training with data from the end of the season in early-season setting.

We validated the models using We validated the models using metrics calculated for four level of aggregation: (i) with all the labels, (ii) with the aggregation of the labels using the Automatic Hierarchical Label Aggregation, (iii) with a set of crop of interest from the aggregation that were recognized important by a Food Security expert and with or (iv) without classes *others* and *grassland* (majority class in NL dataset). We used macro-average of the Precision, Recall and F1-score because the dataset is unbalanced. We also used micro-F1 score (m-F1) for the last setting, because accuracy is not possible when focusing on a subset of the classes. In addition, we computed the Accuracy as a general metric.

4.2. In-country end-of-season results

The results of the various models on France and the NL are shown in Table 4 and Table 5 with respect to four distinct classification schemes, ranging from a fine-grained 141-class scheme for NL (resp. 151 for FR) to a coarse-grained 10-class scheme (resp. 14 for FR). The 8-class scheme (resp. 12 for FR) is the same than the 10-class one, in order to only focus the performances on the crops of interest. Table 4 and Table 5 aim at showing the interest of our multi-modal method compared to what is generally used in the field, by using only the remote sensing of the year, in an independent way.

4.3. In-country early-season results

We compared the performance of the vanilla (i.e. without data-augmentation) models, trained solely on end-of-season classification examples, with in-season models trained using the proposed data-augmentation technique (see Section 3.3). Comparisons were made using all modalities, the model using only remote sensing data for both vanilla and early-season, as well as the model using only crop data. We observed that the vanilla

model performs worse when used for in-season classification, as expected. Fig. 7 shows the performances of the model in terms of micro-F1 on the set of 10 crops. We focused on the results of the model trained using this data-augmentation over the NL.

4.4. Cross-country transfer learning results

Table 6 shows the performance of our best architecture model on the NL. The neural network was trained either from scratch or using a pre-trained model. We compared its performances on a few-shot setting against using the full NL dataset. The table shows that pre-training the model led to improved performance in terms of almost all metrics for all tasks. Furthermore, the performance increases with the number of training examples, and the highest performance was achieved for 1024 training examples for each aggregated class. Notice that the non-pretrained model using $N = All$ corresponds to $HierE_{final}$ from Table 4.

5. Discussion

The results are discussed in the five first subsections of the section, then followed by a presentation of the limitations (Section 5.6) and recommendations for future research (section 5.7).

5.1. The label aggregation method

In line with second objective, we introduced a distinct benchmarking approach that utilizes HCATv2, the hierarchical crop type classification system of EuroCrops. In Table 4 (NL) and Table 5 (FR), the aggregation level is displayed in the 24-class and 32-class columns, respectively. This means that the performance results for both countries incorporate the internal distributions. Overall, the accuracy scores for both countries did not exhibit significant variation when accounting for all EuroCrops classes (93.6 and 85.4, for NL and FR, respectively) or after aggregation (94.0 and 85.7), suggesting that the models performed well on the very dominant classes. However, the macro F1-scores experienced an improvement due to the merging of classes with a limited number of samples: it reveals the interest of the aggregation method for classifier performances evaluation on a dataset with a high number of crop classes.

5.2. Hierarchical multimodal models: a way to gain in performances

The third objective of the study (section 1.2) is to evaluate the performances of models relying on diverse model configurations involving different modalities.

For the NL, the results of Table 4 indicate that the best performance was achieved by the final model ($HierE_{final}$) combining the three modalities. It achieved a macro-F1 score of 40.2% on the 141-class scheme and a micro-F1 score of 91.6% on the 8-class scheme. With the exception of $HierE_{RS}$, which failed to learn (achieving an F1 score of 0 for both the 8- and 12-class settings), all models based on LSTM to process RS time series achieve higher performances compared to the approach of concatenating statistical functional vectors of

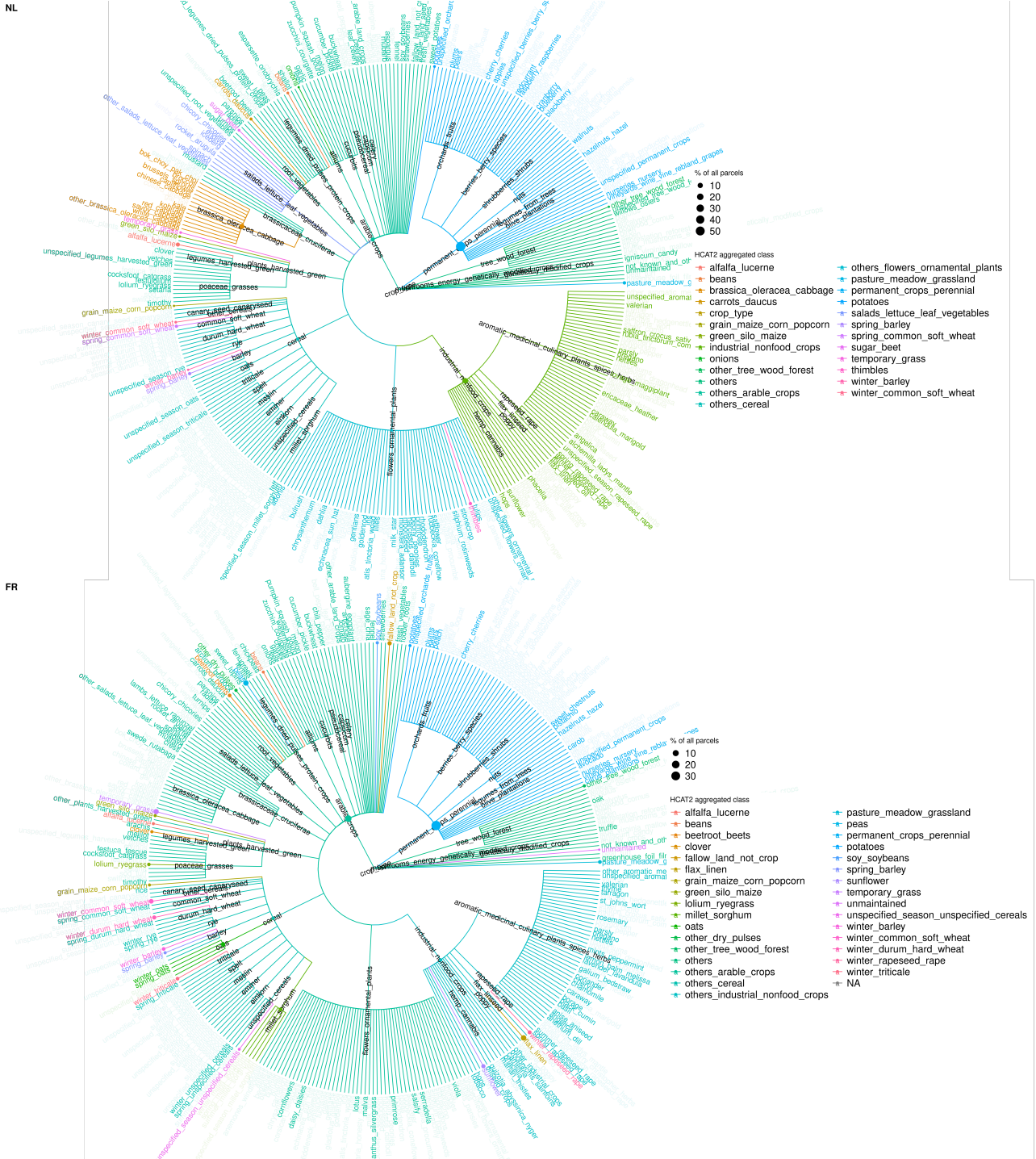


Fig. 6: Aggregated classes selected for validation in each country for FR (A) and NL (B) along with the distribution. The colour highlight the crop type or crop group that were assessed for both country in red and only for one respective country in cyan.

each sliding window. Notably, the unimodal IntraYE_{RS} outperformed InterYE_{RS} , while the multimodal IntraYE_{MM} and HierE_{MM} outperform InterYE_{MM} .

Several similarities and notable differences can be observed when comparing the models between FR (Table 5) and the NL (Table 4). First, the general performance metrics were lower for FR than for the NL. This difference may be attributed to FR having more classes than the NL. Second, the performances of the RS model's performance using only one year of context

(InterYE_{RS}) were significantly lower than for the same one on NL, relatively to the other models. The higher variance of the RS data in FR, resulting from its larger size and greater diversity compared to the NL, may contribute to the lower performances observed in this scenario.

5.3. Performances per crops

The utilization of various modalities and their combinations for each of the primary crops in both countries is depicted in

Labels Model	# Modalities	141-class				24-class				10-class				8-class			
		P	R	F1	Acc	P	R	F1	Acc	P	R	F1	Acc	P	R	F1	m-F1
InterYE _{Crop}	1 (C)	36.0	25.5	27.4	76.2	53.3	37.2	39.1	76.5	51.8	43.0	43.5	77.7	43.3	35.5	34.9	53.6
IntraYE _{RS} 2019b	1 (RS)	27.4	20.9	20.4	89.8	64.0	60.9	60.4	90.3	78.8	75.9	74.5	92.9	76.1	72.6	70.8	87.8
InterYE _{RS}	1 (RS)	22.8	17.7	17.1	89.1	59.2	58.5	57.3	89.6	71.2	73.4	72.0	92.1	67.0	69.6	68.0	85.6
HierE _{RS}	1 (RS)	0.4	0.8	0.6	56.9	2.4	4.2	3.0	56.9	5.7	10.0	7.3	57.4	0.0	0.0	0.0	0.0
IntraYE _{MM} 2021	2 (RS+BoC)	55.6	39.7	43.2	92.8	76.6	69.8	72.1	93.1	83.0	80.5	80.9	94.7	80.2	77.9	78.0	90.0
InterYE _{MM}	2 (RS+C)	41.1	33.0	33.6	92.2	70.8	70.5	69.9	92.6	82.2	79.7	80.4	94.5	80.2	76.3	77.5	89.5
HierE _{MM}	2 (RS+C)	47.3	38.7	39.7	93.3	74.7	75.5	74.7	93.7	85.2	81.9	83.1	95.2	83.6	78.8	80.6	91.1
HierE _{final}	3 (All)	47.1	39.3	40.2	93.6	76.6	75.8	75.7	94.0	86.7	81.9	83.6	95.5	85.3	78.7	81.1	91.6

Table 4: Results over Netherlands of the end-of-season classification models with different modalities: Remote Sensing (RS), Crop Rotations as embeddings (C) or BoC, and Spatial Crop Distribution. The metrics shown are macro Precision (P), Recall (R) and F1 score, as well as accuracy and micro-F1 score (m-F1).

Labels Model	# Modalities	151-class				32-class				14-class				12-class			
		P	R	F1	Acc	P	R	F1	Acc	P	R	F1	Acc	P	R	F1	m-F1
InterYE _{Crop}	1 (C)	35.6	31.0	31.7	66.0	43.7	38.8	38.7	66.2	38.9	34.3	31.7	69.1	30.9	26.4	23.0	42.7
IntraYE _{RS} 2019b	1 (RS)	22.9	15.7	15.2	64.0	51.1	46.0	44.6	64.5	69.8	62.2	64.7	75.7	69.3	59.7	63.1	74.6
InterYE _{RS}	1 (RS)	21.3	13.2	12.6	54.9	46.5	41.5	39.2	55.5	63.9	59.6	60.2	72.2	62.7	57.4	58.5	71.2
HierE _{RS}	1 (RS)	0.1	0.7	0.1	12.4	0.4	3.1	0.7	12.4	1.4	7.1	2.4	19.9	0.0	0.0	0.0	0.0
IntraYE _{MM} 2021	2 (RS+BoC)	52.7	32.4	35.9	82.7	70.1	59.3	61.8	82.8	78.1	68.7	71.0	86.6	76.2	65.6	68.0	80.3
InterYE _{MM}	2 (RS+C)	45.9	35.2	36.4	82.4	67.7	60.5	62.4	82.7	72.7	67.4	69.2	86.1	70.0	63.6	65.8	77.5
HierE _{MM}	2 (RS+C)	50.2	41.9	43.2	84.8	70.7	67.6	68.2	85.0	77.0	73.4	74.9	88.4	75.0	70.2	72.3	81.8
HierE _{final}	3 (All)	45.1	37.3	38.1	85.4	72.1	68.8	69.2	85.7	79.8	76.1	77.6	89.1	78.1	73.5	75.4	83.6

Table 5: Results over France of the end-of-season classification models with different modalities: Remote Sensing (RS), Crop Rotations as embeddings (C) or Bag-of-Crops (BoC), and Spatial Crop Distribution. The metrics shown are macro precision, recall and F1 score, as well as accuracy and micro-F1 score (m-F1).

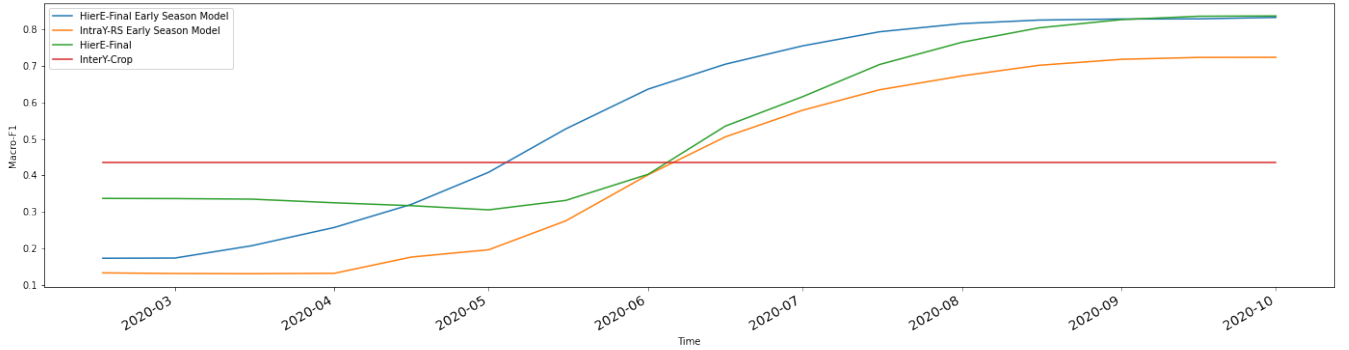


Fig. 7: Comparison of early classification using different modalities, with/out data augmentation (macro-F1 with 10 classes) on Netherlands.

Fig. 9 and Fig. 8. It demonstrated an upward trend in the level of improvement with an increase in the number of modalities employed. The benefits of crop rotation were more significant for certain crops such as pasture, while others such as beetroot are harder to predict without RS signal. The suggested that the crop rotation for FR, limited to only starting from 2015, might not offer enough information to accurately predict crops in complex or irregular crop rotation sequences.

Fig. 10 provides more detailed information on the performance of the best model in the NL and FR. It displays the F1 scores for eight crops of interest in the NL and twelve crops of interest in FR, based on the time of the year used for prediction. Furthermore, for the same crops, we analysed the time series data for the 2020 cropping season (i.e., the test year) averaged at the country level for each of the four remotely sensed variables on Fig. A.2, accompanied by the standard error shown on

Fig. A.3. These visualizations highlight both the variability between crops and the potential confusion that can arise between different crop types.

The end-of-season performances of the models in the NL and FR, denoted as HierE_{final}, are presented using 5km grid cell maps in Fig. 11 and Fig. 12 respectively. The maps reveal notable regional effects, particularly in FR. For instance, in Brittany (located in the north-west of FR), lower accuracy was observed for most crops, especially *winter barley*. It worth noting that despite labeling the crop types uniformly by country, variations in crop varieties, climates, and agricultural practices among farmers have an impact on phenology, consequently affecting the RS signal. Consequently, using a single dataset for training the model resulted in heterogeneous performances over a large country like FR. The development of regional models is thus highly recommended. Furthermore, the model lacks in-

Labels Pre-train.	N	141-class				24-class				10-class				8-class			
		P	R	F1	Acc	P	R	F1	Acc	P	R	F1	Acc	P	R	F1	m-F1
✗	0	∅	∅	∅	∅	∅	∅	∅	∅	∅	∅	∅	∅	∅	∅	∅	∅
	16	5.8	5.1	4.8	70.8	23.7	21.4	20.4	71.1	38.5	37.4	36.3	73.6	38.5	37.4	36.3	45.3
	64	2.7	2.5	2.2	69.2	17.1	13.1	12.5	69.4	27.3	25.7	23.3	69.6	27.3	25.7	23.3	34.7
	256	4.2	4.8	2.9	66.5	18.2	16.9	14.1	66.8	25.0	23.2	20.5	68.1	25.0	23.2	20.5	20.4
	1024	19.6	13.3	12.4	80.8	53.6	39.8	37.2	80.3	69.7	60.4	61.5	84.0	69.7	60.4	61.5	76.3
✓	0	5.7	4.8	4.2	47.3	14.7	15.1	11.1	46.6	20.6	19.7	16.6	46.9	12.3	7.4	8.4	24.5
	16	12.2	7.8	7.6	70.3	30.5	23.8	24.5	70.4	37.9	33.9	34.0	72.3	37.9	33.9	34.0	45.2
	64	16.7	13.6	13.5	74.7	41.9	38.7	38.1	75.0	51.6	45.4	46.6	76.4	51.6	45.4	46.6	54.4
	256	25.8	21.4	20.8	82.5	55.6	51.1	50.6	82.7	67.3	58.0	60.1	84.6	67.3	58.0	60.1	69.2
	1024	32.7	27.3	26.0	84.9	61.3	57.3	54.3	84.9	73.8	72.0	71.6	87.0	73.8	72.0	71.6	80.9
✗	All	47.1	39.2	40.2	93.7	76.6	75.8	75.8	94.0	86.7	81.9	83.6	95.5	85.3	78.7	81.1	91.6
✓	All	42.5	35.3	36.0	92.8	67.3	53.4	55.9	94.2	89.9	82.2	85.3	95.7	88.8	77.6	82.3	91.8

Table 6: Results over Netherlands of the few-shot final classification models, with or without pre-training over France. N represent the number of examples shown per aggregated class on the target dataset. The metrics shown are macro precision, recall and F1 score, as well as accuracy and micro-F1 score (m-F1). N stands for the Few-Shot size.

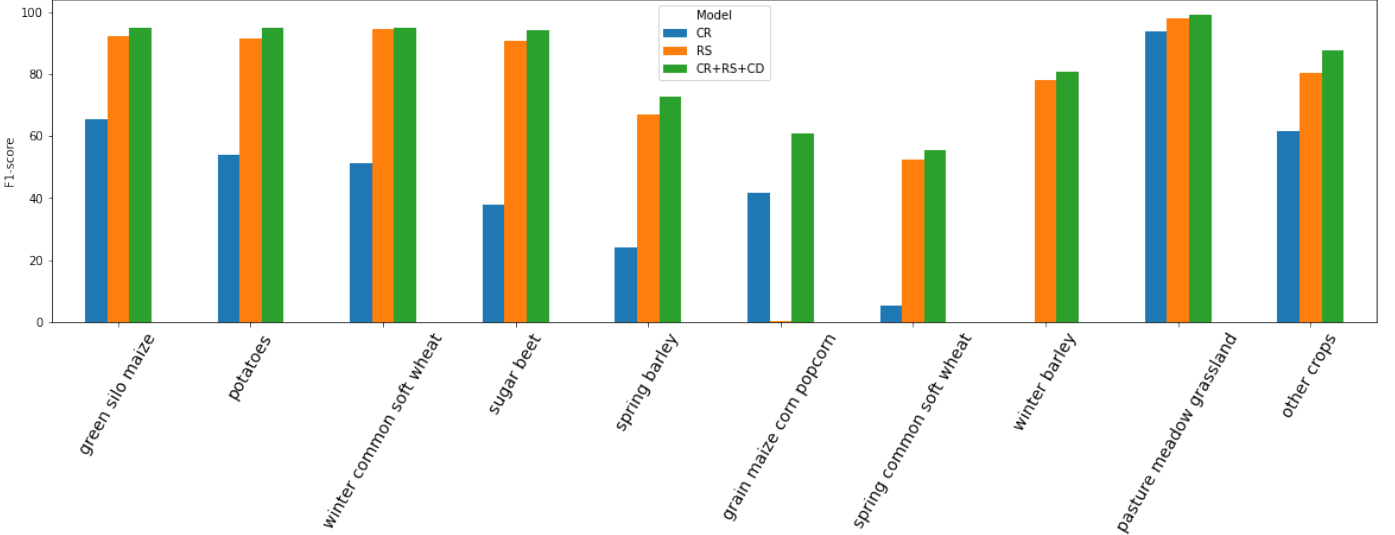


Fig. 8: Comparison of the F1-scores by crops of the best hierarchical multimodal model and the model using different modalities (Crop rotation, Remote sensing only and all) on the Netherlands. We used the InterYE_{Crop} (in blue), IntraYE_{RS} (in orange) and HierE_{final} (in green) models.

formation regarding the specific locations, except through the proxy of crop distribution. Incorporating geographic coordinates and/or weather variables as model inputs could contribute to accounting for spatial variations over large areas, such as FR.

The confusion matrices for both countries can be seen in Fig. 13. These matrices allow for the clustering of crops based on the observed confusions. In general, for both countries, there are instances of crop confusions, indicating misclassifications or difficulties in distinguishing between certain crop types: (i) between *green silo maize* and *grain maize corn popcorn*, (ii) between winter cereals (*winter common soft wheat*, *winter barley*, *winter triticale*), (iii) between spring cereals (*spring barley*, *spring common soft wheat*). These confusions are anticipated as they occur with synchronous phenologies of the crops that could differs significantly from one region to the other in Europe (d’Andrimont et al., 2020, 2021; Meroni et al., 2021).

5.4. Early-season models

The use of sub-setting technique, intended for in-season classification, was found to be ineffective in improving the performance of a model solely trained on remote sensing data, as shown in Fig. 7. However, when the multimodal model including crop rotations was applied, it resulted in improved performances as early as May. It is worth noting that the overall performances of the multimodal model was observed to be inferior to that of a unimodal crop-only model. This was due to the model overemphasizing the RS modality as the season progressed. To address this issue, a gate mechanism could be incorporated, as proposed in Arevalo et al. (2017) and Chen et al. (2017), which selectively discards noisy modalities. By utilizing the multimodal hierarchical configuration, the model achieved around mid-July 95% of the end-of-season overall accuracy. This corresponds to the period when the winter crops are harvested, and the summer crops reach their peak vegeta-

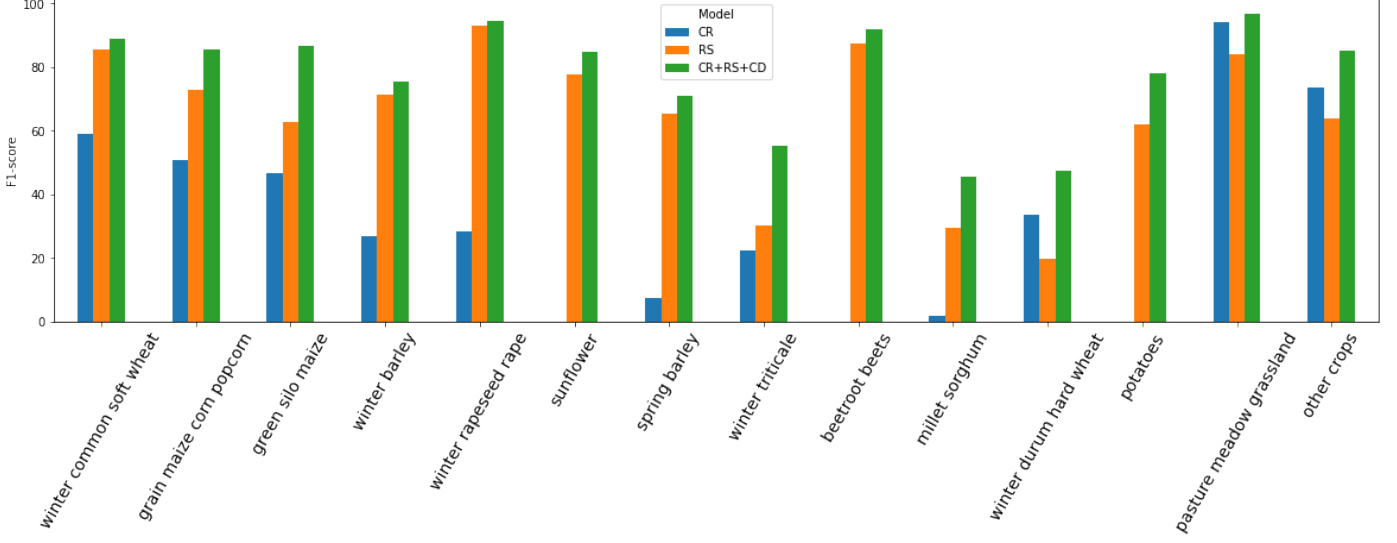


Fig. 9: Comparison of the F1-scores by crops of the best hierarchical multimodal model and the model using different modalities (Crop rotation, Remote sensing only and all) on France We used the $\text{InterYE}_{\text{Crop}}$, $\text{IntraYE}_{\text{RS}}$ and $\text{HierE}_{\text{final}}$ models.

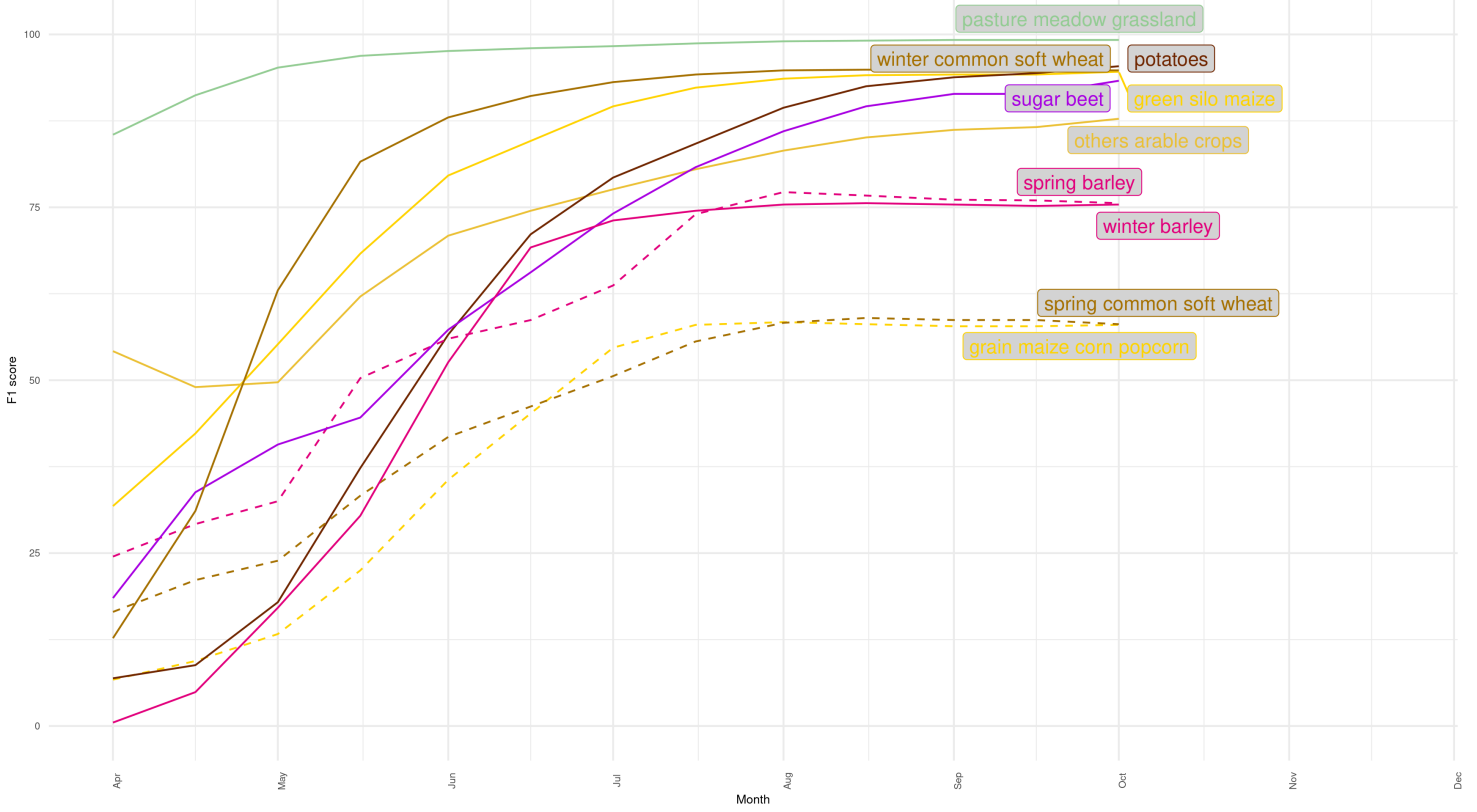


Fig. 10: F1-score per crop group along the season for NL. When crop have winter and spring varieties, the spring varieties are represented as dashed lines.

tion.

In Fig. 10, the HierE_{MM} model data-augmented model was assessed through time. F-score are provided for the 10 classes of interest for NL, as defined in Section 4. Overall, there was an offset of the curve rise-up. The shift is earlier (from mid-April to mid-June), which was consistent with other studies

(Rußwurm et al., 2023).

5.5. Cross-country transfer learning results

According to Table 6, there were two notable distinctions between the models pre-trained on FR and the ones trained from scratch. The first distinction pertained to few-shot setting, where the pre-training enables not only superior but also

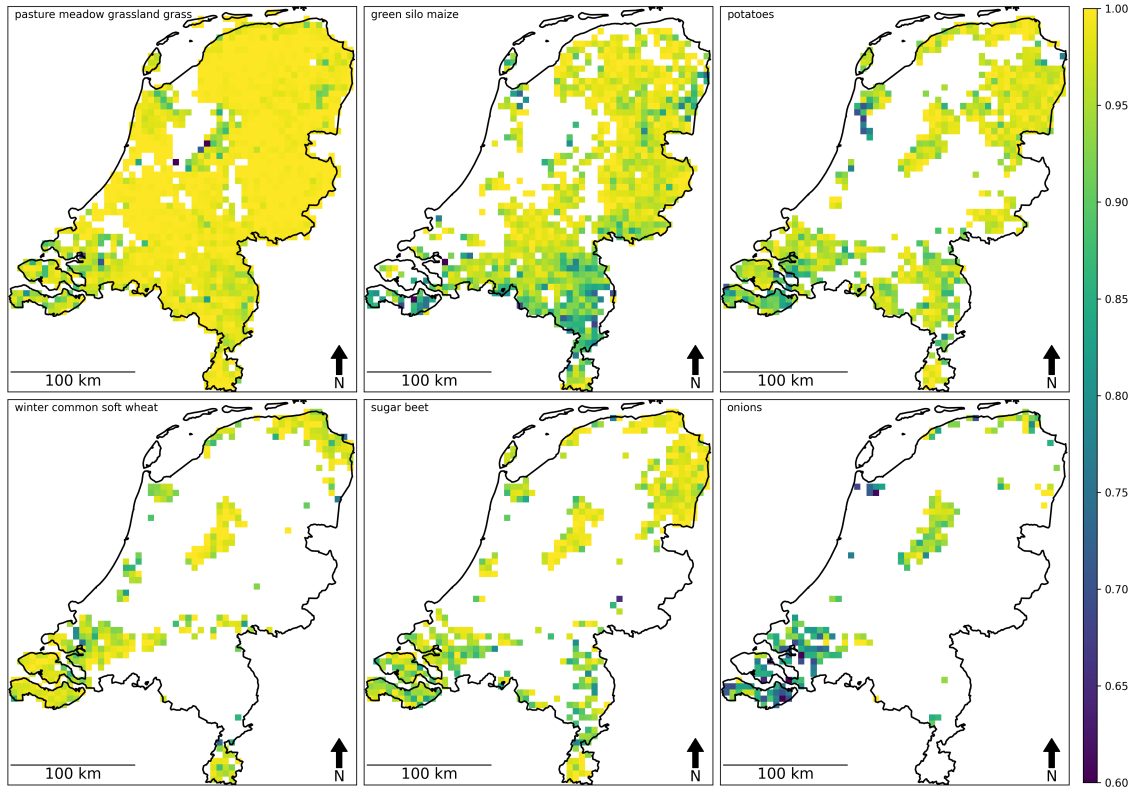


Fig. 11: Map of F1 for the six most important crops over The Netherlands. The F1-score is computed for each crop and for each 5km grid cell. Grid cells with less than 50ha (i.e., 2% of the land) of the given crops are not plotted. Map projection is EPSG:3035.

more consistent results in few-shot classification, reducing dependence on the specific examples used during few-shot training. The second distinction lies in the full-data setting, where we observed that the from-scratch model performs better when validated with 141 and 24 classes (with an m-F1 score of 40.2 and 75.8, respectively, compared to 36.0 and 55.9), while the pre-trained model was better when using fewer classes. This results highlighted an intriguing behaviour, suggesting that the pre-trained neural network was more general and less prone to over-fitted on the prominent classes of the NL dataset. We can conclude that transfer learning proves beneficial when limited labeled examples are available, while in the full-dataset training mode, it enhances the model’s performance for general classes at the expense of specific classes in the dataset.

5.6. Limitations

The primary constraint of this study, particularly in developing countries and numerous other nations, is the requirement for digitized parcel boundary data. Another limitation is the necessity to obtain information regarding the crops cultivated in the previous year. The impact of noisy input data, such as

past crop information derived from a prediction system rather than ground-truth data, remains unknown in terms of the system’s response. Exploring this aspect constitutes an intriguing avenue for future research.

For encoding the RS signal, we utilized a backbone consisting of a mean aggregation of the FOI’s pixels, followed by the application of a temporal context window with statistical functionals. Studies proved that other methods were more efficient in terms of performances (Sainte Fare Garnot et al., 2020). An inherent enhancement to encode the RS signal in a more effective manner would involve employing an end-to-end approach. This approach entails learning the aggregation of RS data and integrating its representation into a neural network, similar to architectures such as CNN-RNN (Pelletier et al., 2019; Sainte Fare Garnot et al., 2019) or more advanced structures like PSE-LTAE (Sainte Fare Garnot et al., 2020; Quinton & Landrieu, 2021; Weilandt et al., 2023). By adopting these powerful architectures, the encoding of RS signals can be optimized, thereby potentially improving the overall performance and accuracy of the system.

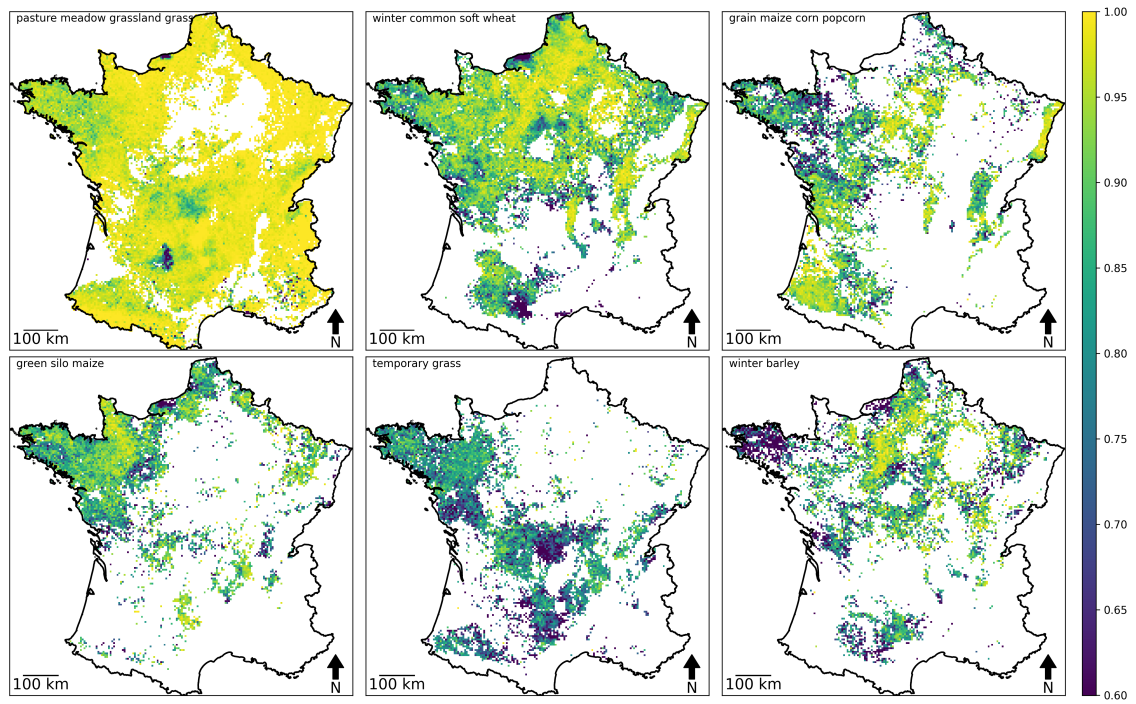


Fig. 12: Map of F1 for the six most import crops over Metropolitan France. See legend of Fig. 11.

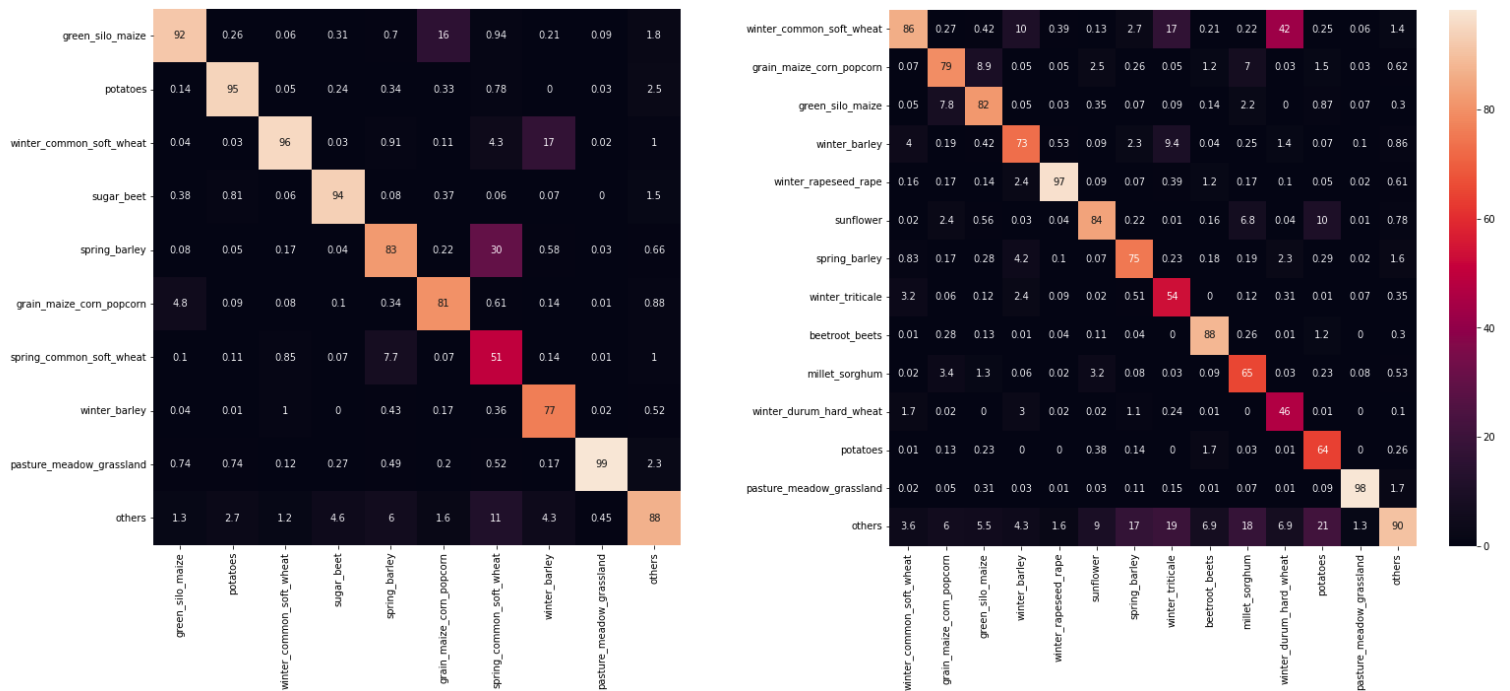


Fig. 13: Confusion matrices for the 10- and 14-class settings for Netherlands and France, respectively.

5.7. Recommendations

Regarding future research directions, there are several avenues for further exploration. One potential direction is to integrate knowledge from the EuroCrop ontology graph inside the learning model, for example by creating multi-level embeddings of each crop. This could improve the ability of the model to capture the complex spatiotemporal variability of crops.

A more complex way to fuse the modalities together could also be explored, such as using a Gated Multimodal Unit (Arevalo et al., 2017). This could lead to better integration of the different data modalities and improved performance of the model.

It would also be valuable to investigate the results at a more regional/local level, especially for FR with its large landmass, crop diversity, and meteorological conditions. Local hierarchical clustering and the performance of the model at the regional level could be examined to gain a deeper understanding of how the model performs in different regions. We saw that the results for FR were lower, possibly due to the diversity of crops and the distribution vector used. Investigating the effect of a region-specialized model, for example by fine-tuning using Adapter layers (Poth et al., 2020), could be a potential solution. In addition, adding meteorological features and investigating their impact could be worthwhile, especially in the case of extreme events. Methods such as Tseng et al. (2021b) or using learned embeddings that represent the time of the thermals (Nyborg et al., 2022) could be explored.

Another area to investigate is the potential of a specific loss function for the early season model, like the one proposed in Rußwurm et al. (2023), as per our simple data-augmentation technique. This could lead to better performance in the early season, which is an ongoing challenge for crop classification.

Other potential avenues for future work include adding more countries to the experiments, but also testing the system with different backbones, allowing ingestion of the EO raw time series as they are. This last step would prevent reliance on man-made filters like Hampel or Whittaker and man-made features like FAPAR and LAI, as they contain filtered information, filtering some that may be useful for the final task (Trigeorgis et al., 2016).

Overall, these future directions could further improve the accuracy and generalization of the proposed multimodal approach for crop classification.

6. Conclusions

In conclusion, we proposed a multimodal hierarchical approach for crop classification that leverages crop rotation history, optical remote sensing signals, and local crop distributions. We released a large harmonized time series dataset of 7M Feature Of Interest (FOI) for a total of around 35M FOI-year. We introduced a new dataset-agnostic method relying on data and expert knowledge for aggregating crops, allowing to evaluate a classifier on a specific region in a meaningful way. Finally, we propose a data-augmentation method to boost the results in early-season setting. Our approach achieved high accuracy

without in-situ data from the test year and showed promising results for cross-domain generalization through transfer learning and few-shot learning experiments. Pre-training on a dataset improves domain adaptation between countries, allowing for cross-domain zero-shot learning and stabilization of the learning in a few-shot setting. Our approach can contribute significantly to agriculture management and policy monitoring.

Author contributions

V.B. and M.C. conceptualized the study. V.B., M.C. and R.D. designed the methodology: M.C. extracted the RS time-series and the original cropcodes on every Feature Of Interest, and proposed to use neural nets on rotations. V.B. proposed hierarchical multimodal models, the hierarchical aggregation, the data-augmentation, the few-shot and transfer learning experiments, extracted the features and ran the experiments. M.S. provided the EuroCrops dataset, harmonisations and support. R.D. helped to formalize all the research. V.B., M.C. and R.D. wrote the draft of the paper. All the authors analyzed the results and wrote the final paper.

Acknowledgements

The authors would like to thank Momtchil Iordanov for his support for visuals and Loic Landrieu for the useful comments on the manuscript. They also would like to thank the Big Data Analytics project for their continuous support. V.B. has been funded by the grant National Center for Artificial Intelligence CENIA FB210017, Basal ANID.

References

- Arevalo, J., Solorio, T., Montes-Y-Gómez, M., & González, F. A. (2017). Gated multimodal units for information fusion. In *5th International Conference on Learning Representations, ICLR 2017 - Workshop Track Proceedings*. [arXiv:1702.01992](https://arxiv.org/abs/1702.01992).
- Bahdanau, D., Chorowski, J., Serdyuk, D., Brakel, P., & Bengio, Y. (2016). End-to-end attention-based large vocabulary speech recognition. *ICASSP, IEEE International Conference on Acoustics, Speech and Signal Processing - Proceedings, 2016-May*, 4945–4949. doi:[10.1109/ICASSP.2016.7472618](https://doi.org/10.1109/ICASSP.2016.7472618). [arXiv:1508.04395](https://arxiv.org/abs/1508.04395).
- Barriere, V. (2017). Hybrid Models for Opinion Analysis in Speech Interactions. In *ICMI* (pp. 647–651).
- Barriere, V., Clavel, C., & Essid, S. (2017). Opinion Dynamics Modeling for Movie Review Transcripts Classification with Hidden Conditional Random Fields. In *INTERSPEECH*.
- Barriere, V., Clavel, C., & Essid, S. (2018). Attitude Classification in Adjacency Pairs of a Human-Agent Interaction with Hidden Conditional Random Fields. In *ICASSP*.
- Barriere, V., & Claverie, M. (2022). Multimodal Crop Type Classification Fusing Multi-Spectral Satellite Time Series with Farmers Crop Rotations and Local Crop Distribution. In *Proceedings of 2nd Workshop on Complex Data Challenges in Earth Observation, IJCAI* (pp. 50–57). volume 3207. [arXiv:2208.10838](https://arxiv.org/abs/2208.10838).
- Benamara, F., Taboada, M., & Mathieu, Y. (2016). Evaluative Language Beyond Bags of Words: Linguistic Insights and Computational Applications. *Computational Linguistics*. URL: <http://www.mitpressjournals.org/doi/10.1162/COLI{ }a{ }00278>. doi:[10.1162/COLI_a_00278](https://doi.org/10.1162/COLI_a_00278). [arXiv:1309.4408](https://arxiv.org/abs/1309.4408).

- Bohan, D. A., Schmucki, R., Abay, A. T., Termansen, M., Bane, M., Charalabidis, A., Cong, R.-G., Derocles, S. A., Dorner, Z., Forster, M., Gibert, C., Harrower, C., Oudoire, G., Therond, O., Young, J., Zalai, M., & Pocock, M. J. (2021). Chapter five - designing farmer-acceptable rotations that assure ecosystem service provision in the face of climate change. In D. A. Bohan, A. J. Dumbrell, & A. J. Vanbergen (Eds.), *The Future of Agricultural Landscapes, Part III* (pp. 169–244). Academic Press volume 65 of *Advances in Ecological Research*. URL: <https://www.sciencedirect.com/science/article/pii/S0065250421000027>. doi:<https://doi.org/10.1016/bs.aecr.2021.01.002>.
- Chen, M., Wang, S., Liang, P. P., Baltrušaitis, T., Zadeh, A., & Morency, L.-P. (2017). Multimodal sentiment analysis with word-level fusion and reinforcement learning. In *Proceedings of the 19th ACM International Conference on Multimodal Interaction* (pp. 163–171).
- Chung, J., Gulcehre, C., Cho, K., & Bengio, Y. (2015). Gated feedback recurrent neural networks. *Proceedings of the 32nd International Conference on Machine Learning, [ICML] 2015*, 37, 2067–2075. URL: <http://arxiv.org/abs/1502.02367>. doi:[10.1145/2661829.2661935](https://doi.org/10.1145/2661829.2661935). arXiv:1502.02367.
- Claverie, M., Ju, J., Masek, J. G., Dungan, J. L., Vermote, E. F., Roger, J.-C., Skakun, S. V., & Justice, C. (2018). The harmonized landsat and sentinel-2 surface reflectance data set. *Remote sensing of environment*, 219, 145–161.
- Claverie, M., Vermote, E. F., Weiss, M., Baret, F., Hagolle, O., & Demarez, V. (2013). Validation of coarse spatial resolution lai and fapar time series over cropland in southwest france. *Remote Sensing of Environment*, 139, 216–230.
- d’Andrimont, R., Claverie, M., Kempeneers, P., Muraro, D., Yordanov, M., Peressutti, D., Batič, M., & Waldner, F. (2023). Ai4boundaries: an open ai-ready dataset to map field boundaries with sentinel-2 and aerial photography. *Earth System Science Data*, 15, 317–329.
- d’Andrimont, R., Taymans, M., Lemoine, G., Ceglar, A., Yordanov, M., & van der Velde, M. (2020). Detecting flowering phenology in oil seed rape parcels with sentinel-1 and -2 time series. *Remote Sensing of Environment*, 239, 111660.
- d’Andrimont, R., Verhegghen, A., Lemoine, G., Kempeneers, P., Meroni, M., & Van der Velde, M. (2021). From parcel to continental scale—a first european crop type map based on sentinel-1 and lucas copernicus in-situ observations. *Remote sensing of environment*, 266, 112708.
- Delloye, C., Weiss, M., & Defourny, P. (2018). Retrieval of the canopy chlorophyll content from sentinel-2 spectral bands to estimate nitrogen uptake in intensive winter wheat cropping systems. *Remote Sensing of Environment*, 216, 245–261.
- Demir, I., Koperski, K., Lindenbaum, D., Pang, G., Huang, J., Basu, S., Hughes, F., Tuia, D., & Raska, R. (2018). DeepGlobe 2018: A challenge to parse the earth through satellite images. *IEEE Computer Society Conference on Computer Vision and Pattern Recognition Workshops, 2018-June*, 172–181. doi:[10.1109/CVPRW.2018.00031](https://doi.org/10.1109/CVPRW.2018.00031). arXiv:1805.06561.
- Dogliotti, S., Rossing, W., & Van Ittersum, M. (2003). Rotat, a tool for systematically generating crop rotations. *European Journal of Agronomy*, 19, 239–250.
- Eilers, P. H., Pesendorfer, V., & Bonifacio, R. (2017). Automatic smoothing of remote sensing data. In *2017 9th International Workshop on the Analysis of Multitemporal Remote Sensing Images (MultiTemp)* (pp. 1–3). IEEE.
- Giordano, S., Bailly, S., Landrieu, L., & Chehata, N. (2020). Improved crop classification with rotation knowledge using sentinel-1 and -2 time series. *Photogrammetric Engineering and Remote Sensing*, 86, 431–441. doi:[10.14358/PERS.86.7.431](https://doi.org/10.14358/PERS.86.7.431).
- Harris, Z. S. (1954). Distributional Structure. *Word*, 10, 146–162. URL: <http://psycnet.apa.org/psycinfo/1956-02807-001>. doi:[10.1007/978-94-009-8467-7_1](https://doi.org/10.1007/978-94-009-8467-7_1).
- Hochreiter, S., & Schmidhuber, J. (1997). LONG SHORT-TERM MEMORY. *Neural Computation*, 9, 1735–1780. URL: <http://www7.informatik.tu-muenchen.de/~hochreit/%5Cnhttp://www.idsia.ch/~juergen>. doi:[10.1162/neco.1997.9.8.1735](https://doi.org/10.1162/neco.1997.9.8.1735). arXiv:1206.2944.
- Johnson, D. M., & Mueller, R. (2021). Pre-and within-season crop type classification trained with archival land cover information. *Remote Sensing of Environment*, 264, 112576.
- Kingma, D., & Ba, J. (2014). Adam: A Method for Stochastic Optimization. *International Conference on Learning Representations*, (pp. 1–13). URL: <http://arxiv.org/abs/1412.6980>. doi:[http://doi.acm.org.ezproxy.lib.ucf.edu/10.1145/1830483.1830503](https://doi.org/http://doi.acm.org.ezproxy.lib.ucf.edu/10.1145/1830483.1830503). arXiv:1412.6980.
- Merlos, F. A., & Hijmans, R. J. (2020). The scale dependency of spatial crop species diversity and its relation to temporal diversity. *Proceedings of the National Academy of Sciences*, 117, 26176–26182.
- Meroni, M., d’Andrimont, R., Vrieling, A., Fasbender, D., Lemoine, G., Rembold, F., Segui, L., & Verhegghen, A. (2021). Comparing land surface phenology of major european crops as derived from sar and multispectral data of sentinel-1 and -2. *Remote sensing of environment*, 253, 112232.
- Mikolov, T., Karafiát, M., Burget, L., Černocký, J., & Khudanpur, S. (2010). Recurrent neural network based language model. In *Eleventh annual conference of the international speech communication association*.
- Nyborg, J., Pelletier, C., & Assent, I. (2022). Generalized Classification of Satellite Image Time Series with Thermal Positional Encoding. *IEEE Computer Society Conference on Computer Vision and Pattern Recognition Workshops, 2022-June*, 1391–1401. doi:[10.1109/CVPRW56347.2022.00145](https://doi.org/10.1109/CVPRW56347.2022.00145). arXiv:2203.09175.
- Osman, J., Inglada, J., & Dejoux, J. F. (2015). Assessment of a Markov logic model of crop rotations for early crop mapping. *Computers and Electronics in Agriculture*, 113, 234–243. doi:[10.1016/j.compag.2015.02.015](https://doi.org/10.1016/j.compag.2015.02.015).
- Paszke, A., Gross, S., Massa, F., Lerer, A., Bradbury, J., Chanan, G., Killeen, T., Lin, Z., Gimelshein, N., Antiga, L., Desmaison, A., Köpf, A., Yang, E., DeVito, Z., Raison, M., Tejani, A., Chilamkurthy, S., Steiner, B., Fang, L., Bai, J., & Chintala, S. (2019). PyTorch: An imperative style, high-performance deep learning library. *Advances in Neural Information Processing Systems*, 32. arXiv:1912.01703.
- Pelletier, C., Webb, G. I., & Petitjean, F. (2019). Temporal convolutional neural network for the classification of satellite image time series. *Remote Sensing*, 11, 1–22. doi:[10.3390/rs11050523](https://doi.org/10.3390/rs11050523). arXiv:1811.10166.
- Peng, K. C., Wu, Z., & Ernst, J. (2018). Zero-Shot Deep Domain Adaptation. *ECCV*, (pp. 793–810). doi:[10.1007/978-3-030-01252-6_47](https://doi.org/10.1007/978-3-030-01252-6_47). arXiv:1707.01922.
- Porter, J., Xie, L., Challinor, A., Cochrane, K., Howden, S., Iqbal, M., Lobell, D., Isabel Travasso, M., Chhetri, N., Garrett, K. et al. (2014). Food security and food production systems, .
- Poth, C., Pfeiffer, J., Andreas, R., Kamath, A., Vuli, I., Ruder, S., Cho, K., & Gurevych, I. (2020). AdapterHub : A Framework for Adapting Transformers. *arXiv preprint arXiv:2007.07779*, .
- Quinton, F., & Landrieu, L. (2021). Crop rotation modeling for deep learning-based parcel classification from satellite time series. *Remote Sensing*, 13. doi:[10.3390/rs13224599](https://doi.org/10.3390/rs13224599). arXiv:2110.08187.
- Rußwurm, M., Courty, N., Emonet, R., Lefèvre, S., Tuia, D., & Tavenard, R. (2023). End-to-end learned early classification of time series for in-season crop type mapping. *ISPRS Journal of Photogrammetry and Remote Sensing*, 196, 445–456. URL: <https://doi.org/10.1016/j.isprsjprs.2022.12.016>. doi:[10.1016/j.isprsjprs.2022.12.016](https://doi.org/10.1016/j.isprsjprs.2022.12.016).
- Rußwurm, M., & Körner, M. (2018). Multi-temporal land cover classification with sequential recurrent encoders. *ISPRS International Journal of Geo-Information*, 7. doi:[10.3390/ijgi7040129](https://doi.org/10.3390/ijgi7040129). arXiv:1802.02080.
- Rußwurm, M., & Körner, M. (2020). Self-attention for raw optical Satellite Time Series Classification. *ISPRS Journal of Photogrammetry and Remote Sensing*, 169, 421–435. doi:[10.1016/j.isprsjprs.2020.06.006](https://doi.org/10.1016/j.isprsjprs.2020.06.006). arXiv:1910.10536.
- Rußwurm, M., Lefèvre, S., Courty, N., Emonet, R., Körner, M., & Tavenard, R. (2019a). End-to-end Learning for Early Classification of Time Series. *Arxiv*, . URL: <http://arxiv.org/abs/1901.10681>. arXiv:1901.10681.
- Rußwurm, M., Lefèvre, S., & Körner, M. (2019b). Breizhcrops: a satellite time series dataset for crop type identification. *Time Series Workshop of the 36th ICML*, .
- Rußwurm, M., Tavenard, R., Lefèvre, S., & Körner, M. (2019c). Early Classification for Agricultural Monitoring from Satellite Time Series. *ICML AI4socialgood workshop*, . URL: <http://arxiv.org/abs/1908.10283>. arXiv:1908.10283.
- Rußwurm, M., Wang, S., Körner, M., & Lobell, D. (2019d). Meta-Learning for Few-Shot Land Cover Classification. In *IEEE/CVF conference on computer vision and pattern recognition workshops*.
- Sainte Fare Garnot, V., Landrieu, L., Giordano, S., & Chehata, N. (2019). Time-Space Tradeoff in Deep Learning Models for Crop Classification on Satellite Multi-Spectral Image Time Series. In *IGARSS* (pp. 6247–6250). doi:[10.1109/IGARSS.2019.8928488](https://doi.org/10.1109/IGARSS.2019.8928488).

- 1109/igarss.2019.8900517. [arXiv:1901.10503](#).
- Sainte Fare Garnot, V., Landrieu, L., Giordano, S., & Chehata, N. (2020). Satellite image time series classification with pixel-set encoders and temporal self-attention. In *Proceedings of the IEEE Computer Society Conference on Computer Vision and Pattern Recognition* (pp. 12322–12331). doi:[10.1109/CVPR42600.2020.01234](#). [arXiv:1911.07757](#).
- Sanh, V., Wolf, T., Ruder, S., Court, H., & Row, H. (2018). A Hierarchical Multi-task Approach for Learning Embeddings from Semantic Tasks. In *AAAI*. [arXiv:arXiv:1811.06031v1](#).
- Schmitt, M., Hughes, L. H., Qiu, C., & Zhu, X. X. (2019). SEN12MS – A CURATED DATASET of GEOREFERENCED MULTI-SPECTRAL SENTINEL-1/2 IMAGERY for DEEP LEARNING and DATA FUSION. *ISPRS Annals of the Photogrammetry, Remote Sensing and Spatial Information Sciences*, 4, 153–160. doi:[10.5194/isprs-annals-IV-2-W7-153-2019](#). [arXiv:1906.07789](#).
- Schneider, M., Broszeit, A., & Körner, M. (2021). Eurocrops: A pan-european dataset for time series crop type classification. *arXiv preprint arXiv:2106.08151*, .
- Schuller, B., Steidl, S., Batliner, A., Hirschberg, J., Burgoon, J. K., Baird, A., Elkins, A., Zhang, Y., Coutinho, E., & Evanini, K. (2016). The INTER-SPEECH 2016 Computational Paralinguistics Challenge: Deception, Sincerity & Native Language. In *Proceedings of the Annual Conference of the International Speech Communication Association, INTERSPEECH*.
- Serban, I. V., Sordoni, A., Bengio, Y., Courville, A., & Pineau, J. (2015). Building End-To-End Dialogue Systems Using Generative Hierarchical Neural Network Models, . URL: <http://arxiv.org/abs/1507.04808>. doi:[10.1017/CBO9781107415324.004](#). [arXiv:1507.04808](#).
- Soille, P., Burger, A., De Marchi, D., Kempeneers, P., Rodriguez, D., Syrris, V., & Vasilev, V. (2018). A versatile data-intensive computing platform for information retrieval from big geospatial data. *Future Generation Computer Systems*, 81, 30–40.
- Trigeorgis, G., Ringeval, F., Brueckner, R., Marchi, E., Nicolaou, M. A., Schuller, B., & Zafeiriou, S. (2016). Adieu features? End-to-end speech emotion recognition using a deep convolutional recurrent network. In *2016 IEEE International Conference on Acoustics, Speech and Signal Processing (ICASSP)* (pp. 5200–5204). URL: <http://ieeexplore.ieee.org/document/7472669/>. doi:[10.1109/ICASSP.2016.7472669](#).
- Tseng, G., Kerner, H., Nakalembe, C., & Becker-Reshef, I. (2021a). Learning to predict crop type from heterogeneous sparse labels using meta-learning. *IEEE Computer Society Conference on Computer Vision and Pattern Recognition Workshops*, (pp. 1111–1120). doi:[10.1109/CVPRW53098.2021.00122](#).
- Tseng, G., Zvonkov, I., Nakalembe, C., & Kerner, H. (2021b). CropHarvest: a global satellite dataset for crop type classification. In *NeurIPS NeurIPS* (pp. 1–14). URL: <https://github.com/nasaharvest/cropharvest>.
- Vaswani, A., Shazeer, N., Parmar, N., Uszkoreit, J., Jones, L., Gomez, A. N., Kaiser, Ł., & Polosukhin, I. (2017). Attention Is All You Need. *arXiv:1706.03762 [cs]*, .
- Weilandt, F., Behling, R., Goncalves, R., Madadi, A., Richter, L., Sanona, T., Spengler, D., & Welsch, J. (2023). Early crop classification via multi-modal satellite data fusion and temporal attention. *Remote Sensing*, 15. URL: <https://www.mdpi.com/2072-4292/15/3/799>. doi:[10.3390/rs15030799](#).
- Weiss, M., & Baret, F. (1999). Evaluation of canopy biophysical variable retrieval performances from the accumulation of large swath satellite data. *Remote sensing of environment*, 70, 293–306.
- Weiss, M., Jacob, F., & Duveiller, G. (2020). Remote sensing for agricultural applications: A meta-review. *Remote sensing of environment*, 236, 111402.
- Xiao, Y., Mignolet, C., Mari, J.-F., & Benoît, M. (2014). Modeling the spatial distribution of crop sequences at a large regional scale using land-cover survey data: A case from france. *Computers and Electronics in Agriculture*, 102, 51–63.
- Xu, C., Tao, D., & Xu, C. (2013). A Survey on Multi-view Learning, . (pp. 1–59). URL: <http://arxiv.org/abs/1304.5634>. doi:[10.1145/1553374.1553391](#). [arXiv:1304.5634](#).
- Yaramasu, R., Bandaru, V., & Phvr, K. (2020). Pre-season crop type mapping using deep neural networks. *Computers and Electronics in Agriculture*, 176, 105664. URL: <https://www.sciencedirect.com/science/article/pii/S0168169920307742>. doi:<https://doi.org/10.1016/j.compag.2020.105664>.

Appendix A

FR / NL crops harmonization (40 crops selected)

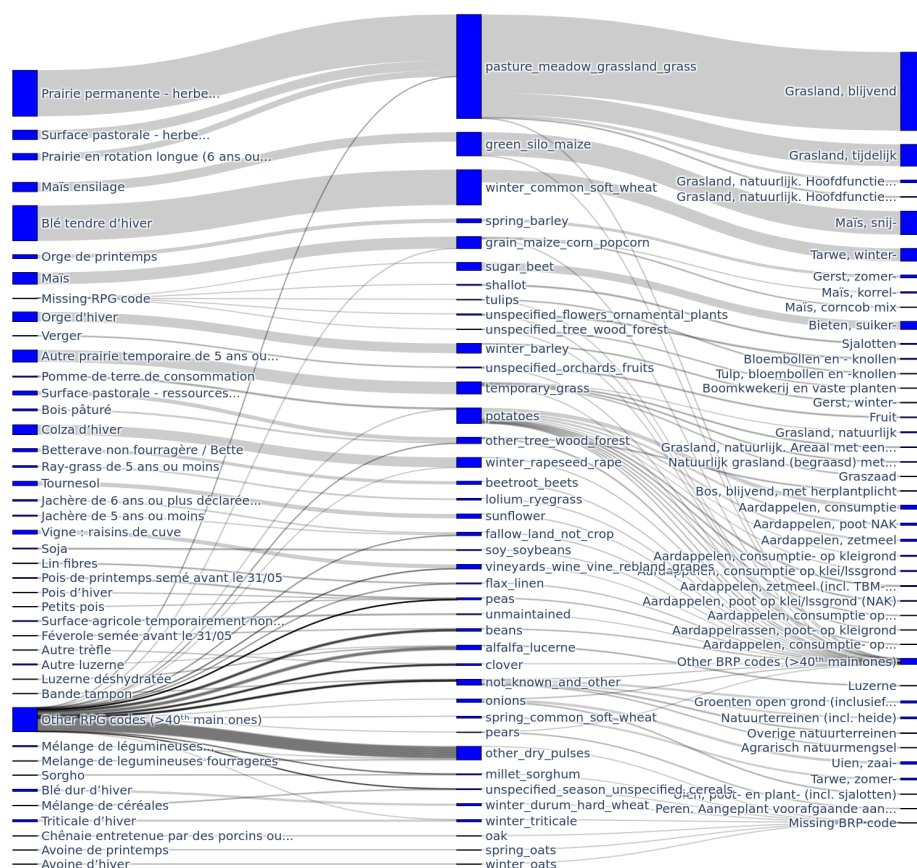


Fig. A.1: Sankey diagram of the crop harmonisation, linking the French RPG (left) and the Dutch BRP (right), using HCATv2 from EuroCrops (center). The bars represent a relative share of the surface for each country. For sake of presentation (in order to fit in one page), only the 40 main crop types for each country are represented. Other crop types are grouped in "Other" classes. An interactive version of the diagram without class limitation is available on https://jeodpp.jrc.ec.europa.eu/ftp/jrc-opendata/DRL/CropDeepTrans/data/sankey_All_crops.html.

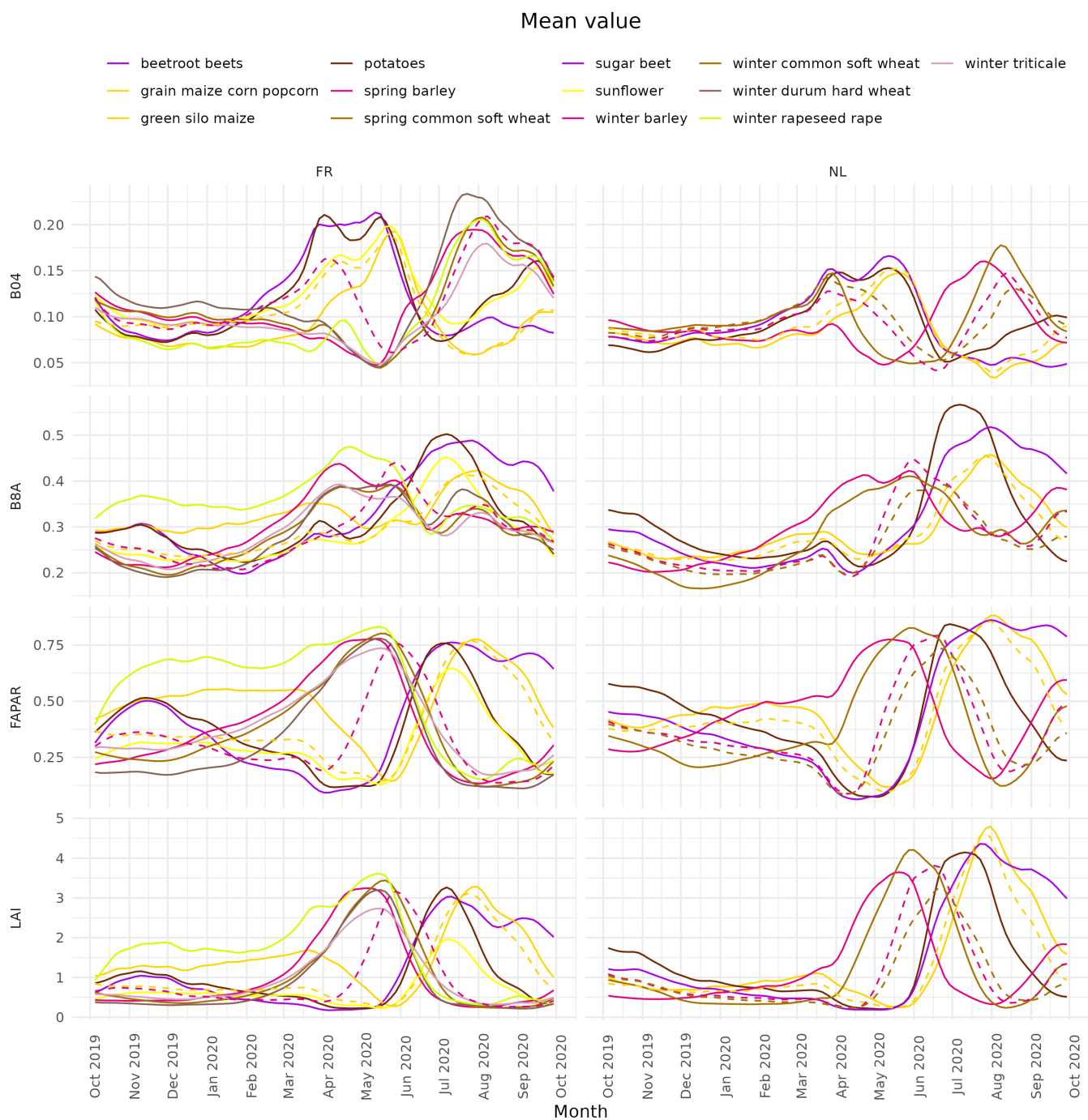


Fig. A.2: Mean of the EO-derived variable for each country 2019-2020. When crop have winter and spring varieties, the spring varieties are represented as dashed lines..

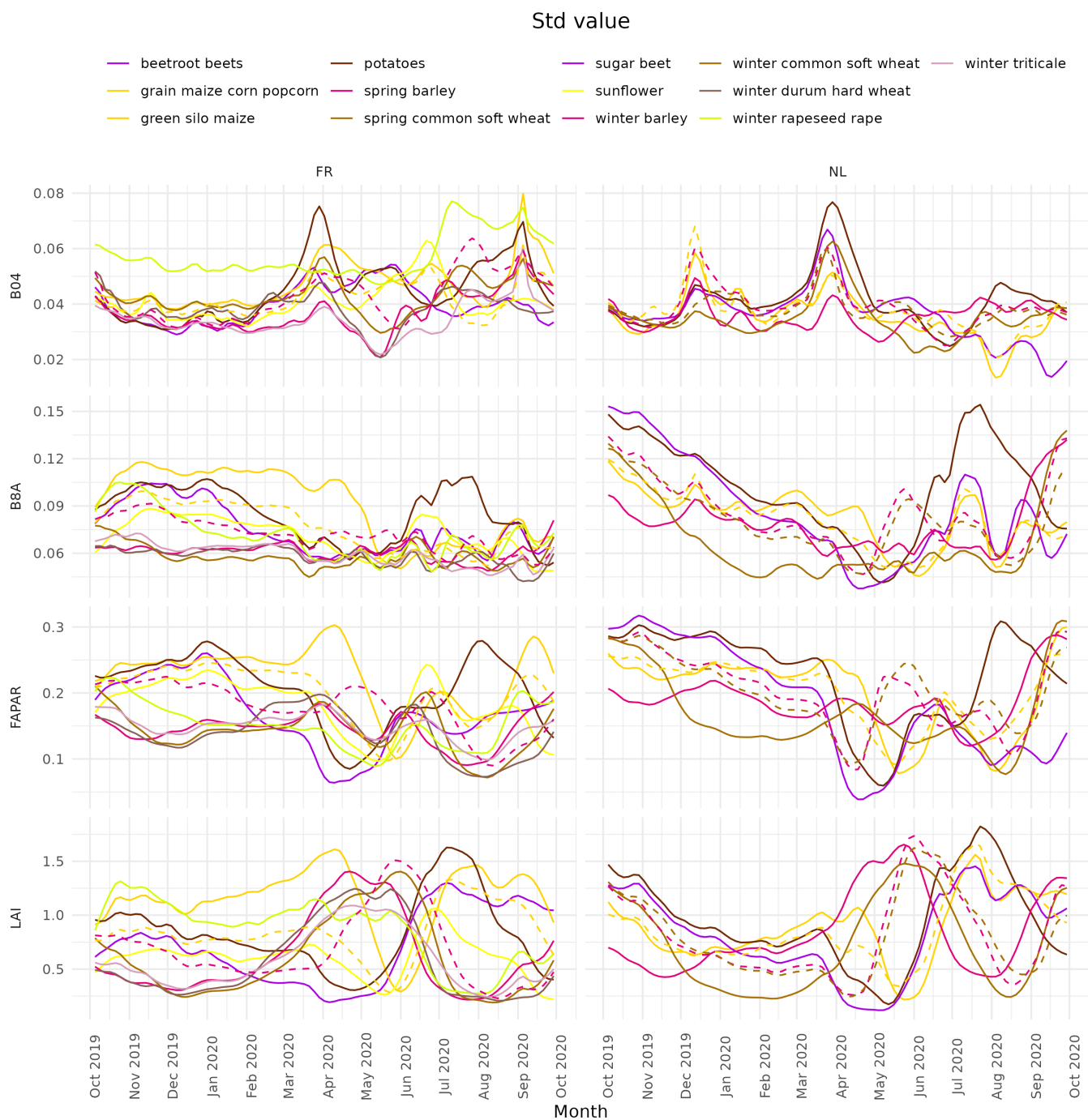


Fig. A.3: Standard deviation of the EO-derived variable for each country for the growing season 2019-2020. When crop have winter and spring varieties, the spring varieties are represented as dashed lines.